

Entropy stable non-oscillatory fluxes: An optimized wedding of entropy conservative flux with non-oscillatory flux

Ritesh Kumar Dubey^{*†1,2}

¹*Research Institute, Department of Mathematics, SRM Institute of Science and Technology, Chennai, India,*

²*Blockapps AI, Bangalore, India*

Abstract

This work settles the problem of constructing entropy stable non-oscillatory (ESNO) fluxes by framing it as a least square optimization problem. A flux sign stability condition is introduced and utilized to construct arbitrary order entropy stable flux as a convex combination of entropy conservative and non-oscillatory flux. This simple approach is robust which does not explicitly requires the computation of costly dissipation operator and high order reconstruction of scaled entropy variable for constructing the diffusion term. The numerical diffusion is optimized in the sense that entropy stable flux reduces to the underlying non-oscillatory flux. Different non-oscillatory entropy stable fluxes are constructed and used to compute the numerical solution of various standard scalar and systems test problems. Computational results show that entropy stable schemes are comparable in term of non-oscillatory nature of schemes using only the underlying non-oscillatory fluxes. Moreover, these entropy stable schemes maintains the formal order of accuracy of the lower order flux used in the convex combination.

Keywords: entropy stability, maximum principle, high order non-oscillatory schemes, sign stability property, Hyperbolic conservation law, Least square optimization.

AMS subject classifications: 65M06, 35L65

1 Introduction

One of the topic of paramount interest in the area of numerical solution of partial differential equations is to design schemes for non-linear hyperbolic systems of conservation laws. These equations are natural models for many physical problems in areas of engineering and scientific studies like gas dynamics, fluid flow problems, astrophysical flow etc. Generic one dimensional system of conservation laws can be written in the form,

$$\frac{\partial \mathbf{u}}{\partial t} + \frac{\partial \mathbf{f}(\mathbf{u})}{\partial x} = 0, \quad \forall (x, t) \in \mathbb{R} \times \mathbb{R}^+, \quad (1)$$

$$\mathbf{u}(x, 0) = \mathbf{u}_0(x), \quad \forall x \in \mathbb{R}. \quad (2)$$

where vector $\mathbf{f}(\mathbf{u}) : \mathbb{R}^m \rightarrow \mathbb{R}^m$ is a smooth flux function of conserved vector quantity $\mathbf{u}(x, t) : \mathbb{R} \times \mathbb{R}^+ \rightarrow \mathbb{R}^m$. It is well known that (1) admits discontinuities like shock and rarefaction in its solution which pose further problems like non-unique weak solutions and non-oscillatory crisp numerical resolution of these discontinuities. In fact some of the well known classical schemes converge to physically incorrect weak solution [34]. On one hand low order schemes yield smeared approximation of discontinuities whereas

^{*}riteshkd@srmist.edu.in, ritesh@blockappsai.com

[†]Ritesh Kumar Dubey acknowledges SERB India for providing necessary funds through EMR project EMR/2016/000394 which supported his travel and stay at during research visit to Blockapps AI, Bangalore.

on other hand uniformly high order schemes exhibit spurious oscillations around such discontinuities. Therefore it is required to devise robust and efficient high order schemes which crisply capture these discontinuities without introducing spurious oscillations. Moreover, one core requirement is that such numerical scheme should yield solution which converge to viscosity solution of (1) [13].

Notably the viscosity solution satisfies two intrinsic properties (i) a maximum principle [64] and (ii) it uniquely satisfies entropy stability inequality [56]. These characteristics of the viscosity solution paved the way for devising modern shock capturing schemes. There is a vast literature on numerical schemes which are designed based on above characteristics of physically acceptable solution. We mention a few foundational as well recent significant work which fall inline with the theme of this paper.

Non-Oscillatory schemes which are designed following the maximum principle are monotone schemes [10], high resolution total variation diminishing (TVD) schemes [23, 30, 53, 58, 63, 64]. Schemes which weakly satisfies maximum principle are arbitrary high order accurate Essentially non-oscillatory (ENO) [51] and weighted ENO [49] schemes, and their modified improved versions in [2, 4, 14, 25, 28, 29, 43, 47] etc. Schemes satisfying the maximum principle ensure non-oscillatory approximation for discontinuities but do not guarantee for convergence to viscosity solution. It is important to note that there are schemes which are entropy stable as well strictly satisfies maximum principle e.g., monotone and TVD schemes in [6, 7, 12, 27, 45] however they are at most first order accurate at solution extrema [39, 40, 55].

Entropy stable fluxes for hyperbolic conservation laws can be obtained by adding numerical diffusion into entropy conservative fluxes [54]. Some of the entropy stable schemes designed following this approach are [1, 1, 8, 9, 9, 11, 12, 15, 16, 27, 54, 60, 62]. Note that, entropy stable schemes guarantee for convergence to viscosity solution but they do not ensure for non-occurrence of oscillations in the vicinity of discontinuities particularly higher order schemes due to absence of suitable numerical diffusion [1]. However, deducing the suitable amount of this additive numerical diffusion such that resulting scheme maintains formal high order of accuracy and yet yields non-oscillatory approximate solution is non-trivial and have been a topic of wide interest and research. The existing approach for constructing high order non-oscillatory entropy stable flux using high order numerical diffusion operator demands for (i) sign stability of the reconstructed scaled entropy variable which is very restrictive (ii) explicit computation of dissipation operator which is costly and problem dependent.

The aim of this work is to construct robust and efficient arbitrary high order non-oscillatory entropy stable scheme for hyperbolic conservation laws (1). This idea is to design non-oscillatory entropy stable fluxes such that additive numerical diffusion (i) is implicitly defined (ii) robust in the sense it does not depends sign property of the high order reconstructions of scaled entropy variable (iii) is optimized in such a way that the non-oscillatory property of entropy stable flux is govern by underlying non-oscillatory flux.

The rest of the paper is as follows: For motivation and completeness of the presentation in section 2, a brief introduction and challenges in the construction of *high order non-oscillatory entropy stable fluxes* are highlighted. In 3, a quick introduction on non-oscillatory fluxes like TVD and ENO/WENO is given. The main contribution of this work is given in section 4 where construction of non-oscillatory entropy stable flux is posed as least square optimization problem and required numerical diffusion is deduced using first order optimality condition. In section 5, a flux sign stability lemma for entropy stability of any flux is given and used to retrospectively analysis some well known entropy stable fluxes. In section 6, numerical results by various designed entropy stable schemes are given and compared. Conclusions are given in section 7.

2 Entropy stable scheme

This section briefly present theory and development of entropy stable schemes and comprehensive details can be found in [56, 57]. On assuming that system (1) is equipped with entropy pair $(\eta(\mathbf{u}), q(\mathbf{u}))$ which symmetrizes the system (1). Then it can be shown that a physical weak solution of (1) uniquely satisfies following entropy inequality

$$\frac{\partial}{\partial t} \eta(\mathbf{u}) + \frac{\partial}{\partial x} q(\mathbf{u}) \leq 0, \quad (3)$$

where entropy function $\eta \equiv \eta(\mathbf{u}) : \mathbb{R}^m \rightarrow \mathbb{R}$ is convex and entropy flux function $q(\mathbf{u}) : \mathbb{R}^m \rightarrow \mathbb{R}$ satisfies the following compatibility relation with entropy variable $\mathbf{v} = \eta_{\mathbf{u}}(\mathbf{u})$

$$\mathbf{v}^T \mathbf{f}_{\mathbf{u}} = q_{\mathbf{u}}^T, \quad (4)$$

By virtue of the convexity of η the mapping $\mathbf{v} \rightarrow \mathbf{u}$ is one-to-one and change of variable $\mathbf{u} = \mathbf{u}(\mathbf{v})$ transforms the system (1) into an equivalent symmetric form

$$\frac{\partial}{\partial t} \mathbf{u}(\mathbf{v}) + \frac{\partial}{\partial x} \mathbf{g}(\mathbf{u}) = 0, \quad \mathbf{g}(\mathbf{v}) = \mathbf{f}(\mathbf{u}(\mathbf{v})). \quad (5)$$

The system (5) is symmetric in the sense the Jacobians of temporal and spatial fluxes of variable \mathbf{v} i.e., $\mathbf{u}(\mathbf{v})$ and $\mathbf{g}(\mathbf{v})$ respectively satisfy

$$H(\mathbf{v}) = \mathbf{u}_{\mathbf{v}}(\mathbf{v}) = H^T(\mathbf{v}) > 0, \quad B(\mathbf{v}) = \mathbf{g}_{\mathbf{v}}(\mathbf{v}) = B^T(\mathbf{v}). \quad (6)$$

Moreover, under (4), the Hessian of an entropy function symmetrizes the system (1) as following holds [56]

$$\eta_{\mathbf{u}\mathbf{u}} A = [\partial \eta_{\mathbf{u}\mathbf{u}} A]^T, \quad A = \frac{\partial f(\mathbf{u})}{\partial \mathbf{u}}. \quad (7)$$

In order to numerically approximate the solution of (1), discretize the spatial domain into intervals $I_i = [x_{i-\frac{1}{2}}, x_{i+\frac{1}{2}}]$ using Cartesian mesh $\{x_i\}_{i \in \mathbb{Z}}$ with mesh size $\Delta x = x_{i+1} - x_i$ such that $x_i = (x_{i+\frac{1}{2}} + x_{i-\frac{1}{2}})/2$. Then the semi-discrete finite difference (or finite volume) conservative scheme to compute the updated solution of (1) is given by

$$\frac{d}{dt} \mathbf{u}_i(t) = -\frac{1}{\Delta x_i} \left(\mathbf{F}_{i+\frac{1}{2}} - \mathbf{F}_{i-\frac{1}{2}} \right), \quad (8)$$

where $\mathbf{u}_i(t) = \mathbf{u}(x_i, t)$ and numerical flux function $\mathbf{F}_{i+\frac{1}{2}}$ satisfies the consistency condition that is $\mathbf{F}(\mathbf{u}, \mathbf{u}, \dots, \mathbf{u}) = \mathbf{f}(\mathbf{u})$. The scheme (8) is said to be entropy conservative if it satisfies the following discrete entropy criterion,

$$\frac{d}{dt} \eta(\mathbf{u}_i(t)) + \frac{1}{\Delta x_i} \left(q_{i+\frac{1}{2}} - q_{i-\frac{1}{2}} \right) = 0, \quad (9)$$

where discrete entropy flux function $q_{i+\frac{1}{2}} = q(\mathbf{u}_{i-\frac{1}{2}}, \dots, \mathbf{u}_{i+\frac{1}{2}})$, $l \in \mathbb{Z}^+$ is consistent with entropy flux function q such that

$$q(\mathbf{u}, \mathbf{u}, \dots, \mathbf{u}) = q(\mathbf{u}). \quad (10)$$

Define the notations for jump and average of a discrete quantity z_i , $i \in \mathbb{Z}$ by $[[z]]_i := z_{i+\frac{1}{2}} - z_{i-\frac{1}{2}}$ and $\bar{z}_{i+\frac{1}{2}} := \frac{1}{2}(z_{i+1} + z_i)$ respectively. Then a foundational approach to construct entropy conservative numerical flux in [54] is as follows.

Theorem 1 *Let a consistent numerical flux $\mathbf{F}_{i+\frac{1}{2}} = \mathbf{F}_{i+\frac{1}{2}}^*$ satisfies*

$$[[\mathbf{v}]]_{i+\frac{1}{2}} \mathbf{F}_{i+\frac{1}{2}}^* = [[\psi]]_{i+\frac{1}{2}}, \quad (11)$$

where ψ is entropy potential given by

$$\psi(\mathbf{v}) = \mathbf{v} \cdot \mathbf{g}(\mathbf{v}) - q(\mathbf{u}(\mathbf{v})). \quad (12)$$

Then the scheme (8) with numerical flux \mathbf{F}^* is second order accurate and entropy conservative i.e., computed solution by scheme satisfies the discrete entropy equality (9) with numerical entropy flux

$$q_{i+\frac{1}{2}} \equiv q_{i+\frac{1}{2}}^*(\mathbf{u}_i, \mathbf{u}_{i+1}) = \bar{\mathbf{v}}_{i+\frac{1}{2}}^T \mathbf{F}_{i+\frac{1}{2}}^* - \bar{\psi}_{i+\frac{1}{2}} \quad (13)$$

The entropy conservative flux \mathbf{F}^* obtained from (11) for scalar problem is unique, though suffers from non uniqueness in the case of the system of conservation laws. However, this non-uniqueness does not severely impact the development of entropy conservative fluxes various hyperbolic systems and exhaustively available second as well arbitrary high order entropy conservative fluxes can be found in [5, 16, 27, 33, 56, 60]. A detailed comparison of various entropy conservative fluxes for Euler equation is given in [42].

2.1 Entropy Stable flux and numerical diffusion

The entropy of the solution of hyperbolic conservation law remains conserved for smooth solution and dissipates across shocks. Therefore, schemes using entropy conservative fluxes allow non-physical oscillations near shock due to absence of numerical diffusion which ensures that computed solution exhibits entropy dissipation. A standard procedure to obtain such dissipative fluxes is by explicitly adding numerical diffusion in to the entropy conservative flux [54, 56]. We state the result therein as follows,

Theorem 2 *Let $\mathbf{D}_{i+\frac{1}{2}} \in \mathbf{R}^m \times \mathbf{R}^m$ be symmetric positive semi-definite i.e., $\mathbf{D}_{i+\frac{1}{2}} \geq 0$ and $\mathbf{F}^* : \mathbf{R}^m \rightarrow \mathbf{R}^m$ be entropy conservative flux then the computed solution by scheme (8) using numerical flux of the form*

$$\hat{\mathbf{F}}_{i+\frac{1}{2}} = \mathbf{F}_{i+\frac{1}{2}}^* - \frac{1}{2} \mathbf{D}_{i+\frac{1}{2}} [[\mathbf{v}]]_{i+\frac{1}{2}}, \quad (14)$$

satisfies the following discrete analog of the entropy inequality (3),

$$\frac{d}{dt} \eta(\mathbf{u}_i(t)) + \frac{1}{\Delta x_i} [\hat{q}_{i+\frac{1}{2}} - \hat{q}_{i-\frac{1}{2}}] \leq 0. \quad (15)$$

where numerical entropy flux $\hat{q}_{i+\frac{1}{2}} = q_{i+\frac{1}{2}}^ - \frac{1}{2} \bar{\mathbf{v}}_{i+\frac{1}{2}}^T \mathbf{D}_{i+\frac{1}{2}} [[\mathbf{v}]]_{i+\frac{1}{2}}$.*

The so defined flux $\hat{\mathbf{F}}_{i+\frac{1}{2}}$ is called entropy stable flux and the term $\frac{1}{2} \mathbf{D}_{i+\frac{1}{2}} [[\mathbf{v}]]_{i+\frac{1}{2}}$ in (14) represents numerical diffusion term. The numerical diffusion term in (14) is constituted by a symmetric positive semi-definite dissipation operator $\mathbf{D}_{i+\frac{1}{2}}$ and the jump in the discrete entropy variable \mathbf{v}_i . Note that "A conservative scheme which contain more numerical viscosity than that present in the entropy conservative one is also entropy stable" [54]. Therefore constructing entropy stable flux $\hat{\mathbf{F}}_{i+\frac{1}{2}}$ can be easily done by using any symmetric $\mathbf{D}_{i+\frac{1}{2}} \geq 0$. However, following caveats are there when it comes to design *high order non-oscillatory entropy stable fluxes*.

2.1.1 Quest for suitable dissipation operator

The dissipation of the numerical entropy determines the discontinuities capturing ability of the underlying scheme. Thus just the positiveness property of dissipation operator $\mathbf{D}_{i+\frac{1}{2}}$ alone is not enough to ensure for truly oscillation free entropy stable scheme. Further, excessive dissipation cause smeared approximation of the discontinuity whereas in absence of sufficient diffusion spurious oscillations may occur in the vicinity of discontinuities. Thus the problem is to determine a suitable diffusion operator $\mathbf{D}_{i+\frac{1}{2}}$ which enables the scheme to yield a crisp resolution of discontinuities. Let $\mathbf{A} = \partial_{\mathbf{u}} \mathbf{f}(\mathbf{u})$ be the Jacobian matrix with complete set of independent eigen vectors such that $\mathbf{A} = \mathbf{R} \mathbf{\Lambda} \mathbf{R}^{-1}$ where $\mathbf{\Lambda}$ is a non-negative diagonal matrix depending on eigenvalues of Jacobian \mathbf{A} and \mathbf{R} is matrix of associated eigenvectors. Then some examples of diffusion operator used in [16] are $\mathbf{D}_{i+\frac{1}{2}} = \tilde{\mathbf{R}}_{i+\frac{1}{2}} \tilde{\mathbf{\Lambda}}_{i+\frac{1}{2}} \tilde{\mathbf{R}}_{i+\frac{1}{2}}^T$ where $\tilde{\mathbf{R}}$ is a scaling of \mathbf{R} such that $\mathbf{u}_{\mathbf{v}} = \tilde{\mathbf{R}} \tilde{\mathbf{R}}^T$ and $\mathbf{A} = \tilde{\mathbf{R}} \mathbf{\Lambda} \tilde{\mathbf{R}}^T$. The subscript $i + \frac{1}{2}$ of $\tilde{\mathbf{R}}$ and $\tilde{\mathbf{\Lambda}}$ denotes an average state at cell interface $x_{i+\frac{1}{2}}$. Two of the choices used for $\mathbf{\Lambda}$ therein are Roe type dissipation operator $\mathbf{\Lambda} = \text{diag}(|\lambda_1|, |\lambda_2|, \dots, |\lambda_m|)$ and Rusanov type dissipation operator $\mathbf{\Lambda} = \max(|\lambda_1|, |\lambda_2|, \dots, |\lambda_m|) \mathbf{I}_{m \times m}$. In [27], entropy consistent diffusion operator *EC1* is proposed using a second and third-order differential terms for Euler equation given as,

$$\mathbf{\Lambda}^{EC1} = |\mathbf{\Lambda}| + \frac{1}{6} |[[\mathbf{\Lambda}_{u \pm a}]]| \quad (16)$$

where $[[\mathbf{\Lambda}]] = \text{diag}([u - a], 0, [u + a])$. However, extension of (16) for general hyperbolic systems is not clear and its non-oscillatory nature depends on the choice of entropy function [12]. A total variation diminishing condition is deduced on \mathbf{D} such that the resulting entropy stable flux (14) ensures for the complete removal of spurious oscillations in [12]. For systems it is defined as,

$$\mathbf{D}_{i+\frac{1}{2}} \geq \max \left(\tilde{\mathbf{R}} |\mathbf{\Lambda}| \tilde{\mathbf{R}}^T + |Q^*|, 0 \right) \quad (17)$$

where the entropy viscosity matrix Q^* in terms of Jacobian $B(\mathbf{v})$ in (6) is given by,

$$Q^* = \int_{-\frac{1}{2}}^{\frac{1}{2}} 2\xi B\left(\mathbf{v}_{i+\frac{1}{2}}(\xi)\right), \quad \mathbf{v}_{i+\frac{1}{2}} = \bar{\mathbf{v}}_{i+\frac{1}{2}} + \xi [[\mathbf{v}]]_{i+\frac{1}{2}} \quad (18)$$

Clearly to obtain diffusion operator in (17), one needs to explicitly calculate entropy viscosity which often may not be tractable. Apart from above the diffusion operator \mathbf{D} in context of Shallow water hydrodynamics equation is given using Cholesky decomposition of matrix $\frac{\partial \mathbf{u}}{\partial \mathbf{v}}$ in [11]. Thus it can be observed that for general system defining and computing \mathbf{D} is a complicated step in designing non-oscillatory entropy stable flux.

2.1.2 Need for sign stable high order reconstruction

Note that irrespective of order of accuracy of flux \mathbf{F}^* , entropy stable schemes with numerical diffusion term $\frac{1}{2}\mathbf{D}_{i+\frac{1}{2}} [[\mathbf{v}]]_{i+\frac{1}{2}}$ are only first order accurate as the jump $[[\mathbf{v}]]_{i+\frac{1}{2}}$ in entropy variable across cell interface $x_{i+\frac{1}{2}}$ is of order Δx . Thus in order to achieve high order entropy stable flux, a suitable reconstruction of the jump in the entropy variable \mathbf{v} is needed as shown in TECNO schemes [16]. More precisely, let \mathbf{v}_i^\pm be $(2k-1)^{th}$ order reconstruction of entropy variable \mathbf{v} , then a $(2k-1)^{th}$ order entropy stable flux is obtained by adding a $(2k-1)^{th}$ order diffusion term to $2k^{th}$ order entropy conservative flux in the form

$$\hat{\mathbf{F}}_{i+\frac{1}{2}} = \mathbf{F}_{i+\frac{1}{2}}^* - \frac{1}{2}\tilde{\mathbf{R}}_{i+\frac{1}{2}}\tilde{\mathbf{\Lambda}}_{i+\frac{1}{2}}\langle\langle\tilde{\mathbf{w}}\rangle\rangle_{i+\frac{1}{2}}, \quad (19)$$

where $\langle\langle\tilde{\mathbf{w}}\rangle\rangle_{i+\frac{1}{2}} = \tilde{\mathbf{w}}_{i+1}^+ - \tilde{\mathbf{w}}_i^-$ is the jump in the reconstructed values of scaled entropy variable $\mathbf{w}_i^\pm = \tilde{\mathbf{R}}_{i+\frac{1}{2}}^T \mathbf{v}_i$ defined as $\tilde{\mathbf{w}}_i^\pm = \tilde{\mathbf{R}}_{i+\frac{1}{2}}^T \mathbf{v}_i^\pm$. It is shown in [16] that flux (19) is entropy stable provided reconstruction of scaled entropy variable satisfies the following component wise sign property at each interface $x_{i+\frac{1}{2}}$,

$$\text{sign}\left(\langle\langle\tilde{\mathbf{w}}\rangle\rangle_{i+\frac{1}{2}}\right) = \text{sign}\left(\langle\langle\mathbf{w}\rangle\rangle_{i+\frac{1}{2}}\right), \quad (20)$$

where

$$\langle\langle\tilde{\mathbf{w}}\rangle\rangle_{i+\frac{1}{2}} = \tilde{\mathbf{w}}_{i+1}^+ - \tilde{\mathbf{w}}_i^- = \tilde{\mathbf{R}}_{i+\frac{1}{2}}^T \mathbf{v}_{i+1}^- - \tilde{\mathbf{R}}_{i+\frac{1}{2}}^T \mathbf{v}_i^+ = \tilde{\mathbf{R}}_{i+\frac{1}{2}}^T \langle\langle\mathbf{v}\rangle\rangle_{i+\frac{1}{2}}, \quad (21)$$

$$\langle\langle\mathbf{w}\rangle\rangle_{i+\frac{1}{2}} = \mathbf{w}_{i+1}^+ - \mathbf{w}_i^- = \tilde{\mathbf{R}}_{i+\frac{1}{2}}^T \mathbf{v}_{i+1} - \tilde{\mathbf{R}}_{i+\frac{1}{2}}^T \mathbf{v}_i = \tilde{\mathbf{R}}_{i+\frac{1}{2}}^T [[\mathbf{v}]]_{i+\frac{1}{2}}. \quad (22)$$

For each component l , (20) is defined as

$$\begin{aligned} \langle\langle w^l \rangle\rangle_{i+\frac{1}{2}} > 0, & \quad \text{then } \langle\langle \tilde{w}^l \rangle\rangle_{i+\frac{1}{2}} \geq 0, \\ \langle\langle w^l \rangle\rangle_{i+\frac{1}{2}} < 0, & \quad \text{then } \langle\langle \tilde{w}^l \rangle\rangle_{i+\frac{1}{2}} \leq 0, \\ \langle\langle w^l \rangle\rangle_{i+\frac{1}{2}} = 0, & \quad \text{then } \langle\langle \tilde{w}^l \rangle\rangle_{i+\frac{1}{2}} = 0. \end{aligned} \quad (23)$$

Note that TeCNO framework [16] for constructing high order non-oscillatory schemes demands for sign stability property (20) in the high order reconstruction and therefore only ENO reconstruction could be used in [17]. Authors in [1] modified the TECNO framework which demands sign stability of scaled entropy variable only accross locally significantly jumps and therefore can work with other high order reconstructions e.g., third order WENO and high order TVD reconstruction. In [11], high-order accurate well-balanced semi-discrete entropy stable schemes are developed for shallow water magnetohydrodynamics by adding diffusion using a switch function proposed in [1]. The construction of suitable dissipation term therein again based on the WENO reconstruction of the scaled entropy variables. Recently in [36] the third order WENO reconstruction of scaled entropy variables is proposed to construct entropy stable schemes for shallow water equations. We remark here that this scaling involve expansive matrix-vector multiplication between scaled matrix $\tilde{\mathbf{R}}$ and entropy vector \mathbf{v} in each cell.

3 Non-Oscillatory Schemes

This section present a quick review of class of prevailing non-oscillatory schemes. Note that, oscillatory approximations for discontinuous solution of (1) can not be considered as admissible solution since it violets the following global maximum principle satisfied by the its physically admissible solution. In scalar case it is given as,

$$\min_x(u_0(x)) \leq u(x, t) \leq \max_x(u_0(x)), \forall(x, t) \in \mathbb{R} \times \mathbb{R}^+. \quad (24)$$

Examples of Maximum principle (24) satisfying schemes are monotone schemes [10], total variation diminishing (TVD) schemes [19, 23, 53, 63]. Apart from these other non-oscillatory schemes which do not strictly follow maximum principle but practically give excellent non-oscillatory numerical results are uniformly non-oscillatory scheme [24], Essentially non-oscillatory (ENO) and weighted ENO schemes [49–51] and references therein. Among these non-oscillatory schemes, ENO and WENO schemes are very attractive as they preserve formal higher order of accuracy unlike monotone and TVD schemes and are well developed now [2–4, 21, 25, 28, 41, 43].

3.1 Non-oscillatory flux

The fluxes corresponding to ENO/WENO schemes relies on high order reconstruction/interpolation of the conserved quantity at cell interface $x_{i+\frac{1}{2}}$. Let $v(x)$, $x \in \Sigma \subset \mathbb{R}$ be a piece-wise continuous function and the domain Σ is partitioned with the grids $\{x_i\}$, $i \in \mathbb{Z}$, and the point values are given by $v_i = v(x_i)$. Then the k -th order ENO interpolation procedure in an arbitrary interval $I_i := [x_{i-\frac{1}{2}}, x_{i+\frac{1}{2}}]$ utilizes $(2k-1)$ grid point stencil and consists of two steps. The first step chooses smoothest stencil among k consecutive points $S_{pref} = \{x_{i-r}, \dots, x_i, \dots, x_{i-r+k-1}\}$ where $r \in \{0, 1, \dots, (k-1)\}$. Then the unique $(k-1)$ -th degree polynomial $p_i(x)$ passing through such S_{pref} is used to interpolate conserved variable at cell interface $x_{i+\frac{1}{2}}$ as,

$$\begin{aligned} v_{i+\frac{1}{2}}^- &= p_i(x_{i+\frac{1}{2}}), \\ v_{i-\frac{1}{2}}^+ &= p_i(x_{i-\frac{1}{2}}). \end{aligned}$$

Compared to ENO, in WENO reconstruction improved accuracy of $(2k-1)^{th}$ order can be achieved using same $(2k-1)$ point stencil for smooth data. The idea in WENO reconstruction is to consider a convex combination of reconstructed values at cell interfaces $x_{i+\frac{1}{2}}$ using all $(k-1)^{th}$ order unique polynomials $p_i^r(x)$ which reconstruct function $v(x)$ over sub stencil $S_r(i) = \{x_{i+r-k+1}, \dots, x_{i+r}\}$, $r = 0, \dots, k-1$ [50]. Such $(2k-1)^{th}$ order accurate reconstructed values are given by

$$v_{i+\frac{1}{2}}^- = \sum_{r=0}^{k-1} \omega_r p_i^r(x_{i+\frac{1}{2}}), \quad v_{i-\frac{1}{2}}^+ = \sum_{r=0}^{k-1} \tilde{\omega}_r p_i^r(x_{i-\frac{1}{2}}). \quad (25)$$

where non-linear weights $\omega_r, \tilde{\omega}_r$ are given by

$$\omega_r = \frac{\alpha_r}{\sum_{p=0}^k \alpha_p}, \quad \tilde{\omega}_r = \frac{\tilde{\alpha}_r}{\sum_{p=0}^k \tilde{\alpha}_p}, \quad (26a)$$

with

$$\alpha_r = \frac{\gamma_r}{(\epsilon + \beta_r)^2}, \quad \tilde{\alpha}_r = \frac{\tilde{\gamma}_r}{(\epsilon + \beta_r)^2}. \quad (26b)$$

The constants γ_r and $\tilde{\gamma}_r$ are such that

$$\sum_{r=0}^{k-1} \gamma_r p_i^r(x_{i+\frac{1}{2}}) - v(x_{i+\frac{1}{2}}) = O(h^{2k-1}),$$

and

$$\sum_{r=0}^{k-1} \tilde{\gamma}_r p_i^r(x_{i-\frac{1}{2}}) - v(x_{i-\frac{1}{2}}) = O(h^{2k-1}).$$

The parameters β_r 's in (26b) measures the smoothness and is given by

$$\beta_r = \sum_{l=1}^k \int_{x_{i-\frac{1}{2}}}^{x_{i+\frac{1}{2}}} \Delta x^{2l-1} \left(\frac{d^l}{dx^l} p_i^j(x) \right)^2 dx, \quad (j = 0, 1, \dots, k-1). \quad (27)$$

A good detail on ENO/WENO reconstruction and interpolation procedure can be found in [17, 49]. In scalar case, the ENO/WENO flux $F_{i+\frac{1}{2}}^s$ in finite difference semi-discrete conservative approximation (8) is reconstructed by point values $f(u_i)$. More precisely, use $f^+(u_i)$ to reconstruct the positive cell interface numerical flux $F_{i+\frac{1}{2}}^+ = v_{i+\frac{1}{2}}^-$ and use $f^-(u_i)$ to reconstruct the negative cell interface numerical flux $F_{i+\frac{1}{2}}^- = v_{i+\frac{1}{2}}^+$. The positive and negative flux f^\pm satisfy $f(u) = f(u)^+ + f(u)^-$ which can be obtained by any suitable flux splitting such that $\frac{f(u)^+}{du} \geq 0$, $\frac{f(u)^-}{du} \leq 0$ [49]. For example the simplest Lax-Friedrichs splitting is,

$$f^\pm(u) = \frac{1}{2}(f(u) \pm \sigma u) \quad (28)$$

where $\sigma = \max_u |f'(u)|$ over the relevant range of u . Finally the non-oscillatory ENO/WENO numerical flux can be obtained by $F_{i+\frac{1}{2}}^s = F_{i+\frac{1}{2}}^+ + F_{i+\frac{1}{2}}^-$. We conclude this section that it can be observed that despite of active efforts to develop high order entropy stable schemes, entropy stable fluxes are never designed to explicitly mimic properties of established aforementioned high order non-oscillatory fluxes.

4 Least square optimization Problem

Through out rest of the paper, vectors functions $\hat{\mathbf{F}}$ and \mathbf{F}^* denote generic numerical entropy stable and entropy conservative flux respectively whereas \mathbf{F}^s denotes non-oscillatory numerical flux function of any stable scheme like monotone, TVD or ENO, WENO schemes etc. More precisely, Let \mathbf{F}^s be consistent numerical flux function of any n^{th} order non-oscillatory finite difference scheme such that

$$\frac{1}{\Delta x} (\mathbf{F}_{i+\frac{1}{2}}^s - \mathbf{F}_{i-\frac{1}{2}}^s) = \mathbf{f}(\mathbf{u})_x|_{x=x_i} + \mathcal{O}(\Delta x^n). \quad (29)$$

Also let \mathbf{F}^* be a m^{th} order consistent entropy conservative flux for (14) such that

$$\frac{1}{\Delta x} (\mathbf{F}_{i+\frac{1}{2}}^* - \mathbf{F}_{i-\frac{1}{2}}^*) = \mathbf{f}(\mathbf{u})_x|_{x=x_i} + \mathcal{O}(\Delta x^m). \quad (30)$$

Further, the scheme with flux \mathbf{F}^* satisfies the discrete entropy equality (9) with some appropriate numerical entropy function q . For example, in $m = 2p^{th}$, $p \in \mathbb{N}$ order entropy conservative schemes [33] the numerical entropy function is

$$q_{i+\frac{1}{2}} = \sum_{k=1}^p \alpha_k^p \sum_{l=1}^{k-1} q_{i+\frac{1}{2}}^*(\mathbf{u}_{i-l}, \mathbf{u}_{i-l+k}), \quad (31)$$

where q^* is second order numerical entropy flux function (13) and α_k^p 's solve the linear system

$$\sum_{k=1}^p k \alpha_k^p = 1, \quad \sum_{i=1}^p i^{2j-1} \alpha_k^p = 0, \quad (j = 2, 3, \dots, p). \quad (32)$$

Note that for problem (1), these numerical fluxes are discrete vector functions $\hat{\mathbf{F}}_{i+\frac{1}{2}} : \mathbb{R}^m \rightarrow \mathbb{R}^m$, $\mathbf{F}_{i+\frac{1}{2}}^* : \mathbb{R}^m \rightarrow \mathbb{R}^m$, and $\mathbf{F}_{i+\frac{1}{2}}^s : \mathbb{R}^m \rightarrow \mathbb{R}^m$. Denote by \mathbb{P} the set of symmetric positive definite matrices

$\mathbf{A} \in \mathbb{R}^{m \times m}$ s.t. $\mathbf{x}^T \mathbf{A} \mathbf{x} \geq 0, \forall \mathbf{x} \in \mathbb{R}^m$ and $D_{i,j}$ represents $(i,j)^{th}$ element of matrix $\mathbf{D}_{i+\frac{1}{2}}$. Further, denote by $\nabla_{\mathbf{D}}$ the matrix differentiation operator with respect to matrix $\mathbf{D}_{i+\frac{1}{2}}$ defined either in ω or α -derivative sense [38]. We prefer to use ω -derivative definition however the arguments used in the following part of this section hold true for α -derivative definition too. On dropping out the sub-script $i + \frac{1}{2}$ in \mathbf{D} , the ω -derivative of any $n \times q$ matrix function \mathbf{G} w.r. to $m \times m$ matrix \mathbf{D} is defined as

$$\nabla_{\mathbf{D}}^{\omega} \mathbf{G}(\mathbf{D}) = \begin{pmatrix} \frac{\partial \mathbf{G}(\mathbf{D})}{\partial D_{1,1}} & \frac{\partial \mathbf{G}(\mathbf{D})}{\partial D_{1,2}} & \cdots & \frac{\partial \mathbf{G}(\mathbf{D})}{\partial D_{1,m}} \\ \frac{\partial \mathbf{G}(\mathbf{D})}{\partial D_{2,1}} & \frac{\partial \mathbf{G}(\mathbf{D})}{\partial D_{2,2}} & \cdots & \frac{\partial \mathbf{G}(\mathbf{D})}{\partial D_{2,m}} \\ \vdots & \vdots & \ddots & \vdots \\ \frac{\partial \mathbf{G}(\mathbf{D})}{\partial D_{m,1}} & \frac{\partial \mathbf{G}(\mathbf{D})}{\partial D_{m,2}} & \cdots & \frac{\partial \mathbf{G}(\mathbf{D})}{\partial D_{m,m}} \end{pmatrix}_{mn \times qm}, \quad (33)$$

where

$$\frac{\partial \mathbf{G}(\mathbf{D})}{\partial D_{i,j}} = \begin{pmatrix} \frac{\partial \mathbf{G}_{1,1}}{\partial D_{i,j}} & \frac{\partial \mathbf{G}_{1,2}}{\partial D_{i,j}} & \cdots & \frac{\partial \mathbf{G}_{1,q}}{\partial D_{i,j}} \\ \frac{\partial \mathbf{G}_{2,1}}{\partial D_{i,j}} & \frac{\partial \mathbf{G}_{2,2}}{\partial D_{i,j}} & \cdots & \frac{\partial \mathbf{G}_{2,q}}{\partial D_{i,j}} \\ \vdots & \vdots & \ddots & \vdots \\ \frac{\partial \mathbf{G}_{n,1}}{\partial D_{i,j}} & \frac{\partial \mathbf{G}_{n,2}}{\partial D_{i,j}} & \cdots & \frac{\partial \mathbf{G}_{n,q}}{\partial D_{i,j}} \end{pmatrix}_{n \times q}, \quad (34)$$

In this setting, the problem of constructing entropy stable flux $\hat{\mathbf{F}}_{i+\frac{1}{2}}$ in (14) which can imitate non-oscillatory property of $\mathbf{F}_{i+\frac{1}{2}}^s$ can be posed as following modified least square problem i.e.,

$$\mathcal{P}1 : \text{Given } [[\mathbf{v}]]_{i+\frac{1}{2}} \in \mathbb{R}^m, \text{ find matrix } \mathbf{D}_{i+\frac{1}{2}} \in \mathbb{P} \subset \mathbb{R}^m \times \mathbb{R}^m \text{ s.t. } \frac{1}{2} \mathbf{D}_{i+\frac{1}{2}} [[\mathbf{v}]]_{i+\frac{1}{2}} = \mathbf{F}_{i+\frac{1}{2}}^* - \mathbf{F}_{i+\frac{1}{2}}^s.$$

It can be reformulated as following equivalent minimization problems

$$\mathcal{P}2 : \min_{\mathbf{D} \in \mathbb{P}} \|\hat{\mathbf{F}}_{i+\frac{1}{2}} - \mathbf{F}_{i+\frac{1}{2}}^s\| \iff \min_{\mathbf{D} \in \mathbb{P}} \|\hat{\mathbf{F}}_{i+\frac{1}{2}} - \mathbf{F}_{i+\frac{1}{2}}^s\|^2 \quad (35)$$

Deducing such minimizing \mathbf{D} can equivalently written as optimization problem

$$\mathcal{P}3 : \mathbf{D} = \arg \min_{\mathbf{D}_{i+\frac{1}{2}} \in \mathbb{P}} J(\mathbf{D}_{i+\frac{1}{2}}) \text{ where } J(\mathbf{D}_{i+\frac{1}{2}}) = \frac{1}{2} \left(\mathbf{F}_{i+\frac{1}{2}}^* - \frac{1}{2} \mathbf{D}_{i+\frac{1}{2}} [[\mathbf{v}]]_{i+\frac{1}{2}} - \mathbf{F}_{i+\frac{1}{2}}^s \right)^2, \quad (36)$$

where $J(\mathbf{D}_{i+\frac{1}{2}})$ is cost or penalty function. Thanks to convexity of $J(\mathbf{D}_{i+\frac{1}{2}})$ a unique minimizer $\mathbf{D}_{i+\frac{1}{2}}$ exists and can be determined by using the first order optimality condition. Differentiating $J(\mathbf{D})$ w.r.to. matrix \mathbf{D} in ω -derivative sense we have,

$$\nabla_{\mathbf{D}_{i+\frac{1}{2}}} J(\mathbf{D}) = \left(\mathbf{F}_{i+\frac{1}{2}}^* - \frac{1}{2} \mathbf{D}_{i+\frac{1}{2}} [[\mathbf{v}]]_{i+\frac{1}{2}} - \mathbf{F}_{i+\frac{1}{2}}^s \right) \left(-\frac{1}{2} \nabla_{\mathbf{D}_{i+\frac{1}{2}}} (\mathbf{D}_{i+\frac{1}{2}} [[\mathbf{v}]]_{i+\frac{1}{2}}) \right) \quad (37)$$

Note that the tensor $\nabla_{\mathbf{D}_{i+\frac{1}{2}}} (\mathbf{D}_{i+\frac{1}{2}} [[\mathbf{v}]]_{i+\frac{1}{2}}) \not\equiv \mathbf{0}$ identically until $[[\mathbf{v}]]_{i+\frac{1}{2}} = \mathbf{0}$ and in this case entropy stability can be achieved trivially in (14). Thus first order sufficient optimality condition i.e., $\nabla_{\mathbf{D}_{i+\frac{1}{2}}} J(\mathbf{D}) = 0$ gives the following condition on minimizing optimizer \mathbf{D}^o

$$\frac{1}{2} \mathbf{D}_{i+\frac{1}{2}}^o [[\mathbf{v}]]_{i+\frac{1}{2}} = \mathbf{F}_{i+\frac{1}{2}}^* - \mathbf{F}_{i+\frac{1}{2}}^s \quad (38)$$

Note that solving (38) to explicitly obtain minimizing \mathbf{D}^o in system case is non-trivial. However, the good thing to be observed from (14) the explicit computation of minimizing \mathbf{D}^o is not needed and diffusion term $\frac{1}{2} \mathbf{D}_{i+\frac{1}{2}}^o [[\mathbf{v}]]_{i+\frac{1}{2}}$ can be directly replaced by right hand side expression of (38). However, to ensure entropy stability of the flux the positivity condition $\mathbf{D}^o \geq 0$ holds provided,

$$\text{sign} \left(\mathbf{F}_{i+\frac{1}{2}}^* - \mathbf{F}_{i+\frac{1}{2}}^s \right) = \text{sign} \left([[\mathbf{v}]]_{i+\frac{1}{2}} \right). \quad (39)$$

We termed condition (39) as *flux sign stability property*. Therefore, define the *optimized non-oscillatory numerical diffusion* for constructing entropy stable flux (14) as

$$\frac{1}{2}\mathbf{D}_{i+\frac{1}{2}}^o [[\mathbf{v}]]_{i+\frac{1}{2}} = \begin{cases} \mathbf{F}_{i+\frac{1}{2}}^* - \mathbf{F}_{i+\frac{1}{2}}^s & \text{if } \text{sign}(\mathbf{F}_{i+\frac{1}{2}}^* - \mathbf{F}_{i+\frac{1}{2}}^s) = \text{sign}([[\mathbf{v}]]_{i+\frac{1}{2}}), \\ \mathbf{0} & \text{else.} \end{cases} \quad (40)$$

Alternatively the entropy stable flux $\hat{\mathbf{F}}_{i+\frac{1}{2}}$ can be expressed as following convex combination

$$\hat{\mathbf{F}}_{i+\frac{1}{2}} = \mathbf{F}_{i+\frac{1}{2}}^* - \chi_{i+\frac{1}{2}} (\mathbf{F}_{i+\frac{1}{2}}^* - \mathbf{F}_{i+\frac{1}{2}}^s), \quad (41)$$

where

$$\chi_{i+\frac{1}{2}} = \begin{cases} 1 & \text{if } \text{sign}(\mathbf{F}_{i+\frac{1}{2}}^* - \mathbf{F}_{i+\frac{1}{2}}^s) = \text{sign}([[\mathbf{v}]]_{i+\frac{1}{2}}), \\ 0 & \text{else.} \end{cases}$$

Theorem 3 *The numerical scheme with flux (14) with numerical diffusion (40) is entropy stable and its solution satisfies*

$$\frac{d}{dt}\eta(\mathbf{u}_i(t)) + \frac{1}{\Delta x_i} [\hat{q}_{i+\frac{1}{2}} - \hat{q}_{i-\frac{1}{2}}] \leq 0 \quad (42)$$

where discrete entropy function $\hat{q}_{i+\frac{1}{2}} = q_{i+\frac{1}{2}}^* - \frac{1}{2}\bar{\mathbf{v}}_{i+\frac{1}{2}}^T \mathbf{D}_{i+\frac{1}{2}}^o [[\mathbf{v}]]_{i+\frac{1}{2}}$ and $q_{i+\frac{1}{2}}^*$ is the numerical entropy flux associated with the entropy conservative flux $\mathbf{F}_{i+\frac{1}{2}}^*$.

Proof: It follows from (40) that

$$[[\mathbf{v}]]_{i+\frac{1}{2}}^T \mathbf{D}_{i+\frac{1}{2}}^o [[\mathbf{v}]]_{i+\frac{1}{2}} = \begin{cases} [[\mathbf{v}]]_{i+\frac{1}{2}}^T (\mathbf{F}_{i+\frac{1}{2}}^* - \mathbf{F}_{i+\frac{1}{2}}^s) & \text{if } \text{sign}([[\mathbf{v}]]_{i+\frac{1}{2}}) = \text{sign}(\mathbf{F}_{i+\frac{1}{2}}^* - \mathbf{F}_{i+\frac{1}{2}}^s) \\ [\mathbf{v}]_{i+\frac{1}{2}}^T \cdot \mathbf{0} & \text{else} \end{cases} \geq 0 \quad (43)$$

Now on multiplying the scheme (8) with \mathbf{v}^T and following the steps in [54] we get

$$\begin{aligned} \frac{d}{dt}\eta(\mathbf{u}_i(t)) + \frac{1}{\Delta x_i} [\hat{q}_{i+\frac{1}{2}} - \hat{q}_{i-\frac{1}{2}}] &= -\frac{1}{4\Delta x} ([[\mathbf{v}]]_{i+\frac{1}{2}}^T \mathbf{D}_{i+\frac{1}{2}}^o [[\mathbf{v}]]_{i+\frac{1}{2}} + [[\mathbf{v}]]_{i-\frac{1}{2}}^T \mathbf{D}_{i-\frac{1}{2}}^o [[\mathbf{v}]]_{i-\frac{1}{2}}) \\ &\leq 0 \end{aligned}$$

□

5 Non-oscillatory Entropy stable flux

On applying Mean value theorem on convex entropy variable $\mathbf{v}(\mathbf{u})$ gives

$$[[\mathbf{v}]]_{i+\frac{1}{2}} = \mathbf{v}_{\mathbf{u}}(\xi) [[\mathbf{u}]]_{i+\frac{1}{2}}, \quad (44)$$

where $\xi \in [\mathbf{u}_i, \mathbf{u}_{i+1}]$ and since $\mathbf{v}_{\mathbf{u}}(\xi) = \eta_{\mathbf{u}\mathbf{u}}(\xi) \geq 0$ it follows,

$$\text{sign}([[\mathbf{v}]]_{i+\frac{1}{2}}) = \text{sign}([[\mathbf{u}]]_{i+\frac{1}{2}}) \quad (45)$$

Thus the non-oscillatory entropy stable flux can be defined in the following simple form

$$\hat{\mathbf{F}}_{i+\frac{1}{2}} = \begin{cases} \mathbf{F}_{i+\frac{1}{2}}^s & \text{if } \text{sign}([[\mathbf{u}]]_{i+\frac{1}{2}}) = \text{sign}(\mathbf{F}_{i+\frac{1}{2}}^* - \mathbf{F}_{i+\frac{1}{2}}^s) \\ \mathbf{F}_{i+\frac{1}{2}}^* & \text{else} \end{cases} \quad (46)$$

Following Lemma which trivially follows provides a *flux sign stability property* for entropy stability of a given flux .

Lemma 4 Let \mathbf{F} be any consistent numerical flux for (1) and if there exist an consistent entropy conservative flux \mathbf{F}^* for (1) such that

$$\mathbf{F}_{i+\frac{1}{2}} = \mathbf{F}_{i+\frac{1}{2}}^* - \frac{1}{2} \tilde{\mathbf{D}}_{i+\frac{1}{2}} [[\mathbf{v}]]_{i+\frac{1}{2}}, \quad (47)$$

where $\tilde{\mathbf{D}}_{i+\frac{1}{2}}$ is any unknown scaling factor then \mathbf{F} is entropy stable provided it satisfies the flux sign stability property holds

$$\text{sign} \left(\mathbf{F}_{i+\frac{1}{2}}^* - \mathbf{F}_{i+\frac{1}{2}}^s \right) = \text{sign} \left([[\mathbf{u}]]_{i+\frac{1}{2}} \right) \quad (48)$$

Proof: Rewrite (47) as

$$\mathbf{F}_{i+\frac{1}{2}}^* - \mathbf{F}_{i+\frac{1}{2}} = \frac{1}{2} \tilde{\mathbf{D}}_{i+\frac{1}{2}} [[\mathbf{v}]]_{i+\frac{1}{2}}, \quad (49)$$

Clearly under the flux sign stability conditions (48) and sign relation (45), scaling factor $\tilde{\mathbf{D}}_{i+\frac{1}{2}} \geq 0$ therefore flux (47) is entropy stable from Theorem 2. \square

In the following we retrospective test the Lemma 4 for some well known entropy stable fluxes.

5.1 First order Entropy stable flux

We remark that the first order entropy stable fluxes in [12, 27], are of the form (47) and under (45) naturally satisfies flux sign stability condition (48) for the dissipation operators characterize by (16) or (17). We further consider the following flux of a generic three point conservative scheme,

$$\mathbf{F}_{i+\frac{1}{2}} = \bar{\mathbf{f}}_{i+\frac{1}{2}} - \frac{1}{2} \alpha_{i+\frac{1}{2}} [[\mathbf{u}]]_{i+\frac{1}{2}} \quad (50)$$

On writing the second order entropy conservative flux (11) in viscosity form [56],

$$\mathbf{F}_{i+\frac{1}{2}}^* = \bar{\mathbf{f}}_{i+\frac{1}{2}} - \frac{1}{2} Q_{i+\frac{1}{2}}^* [[\mathbf{v}]]_{i+\frac{1}{2}} \quad (51)$$

where Q^* is defined in (18). Note from (5) that

$$[[\mathbf{u}]]_{i+\frac{1}{2}} = \int_{\xi=-1/2}^{1/2} \frac{d}{d\xi} \mathbf{u}(\mathbf{v}_{i+\frac{1}{2}}(\xi)) d\xi = \int_{\xi=-1/2}^{1/2} H(v_{i+\frac{1}{2}}(\xi)) d\xi \cdot [[\mathbf{v}]]_{i+\frac{1}{2}} \quad (52)$$

Thus using $\alpha_{i+\frac{1}{2}} [[\mathbf{u}]]_{i+\frac{1}{2}} = Q_{i+\frac{1}{2}} [[\mathbf{v}]]_{i+\frac{1}{2}}$, flux (50) can be written in terms of entropy variable,

$$\mathbf{F} = \bar{\mathbf{f}}_{i+\frac{1}{2}} - \frac{1}{2} Q_{i+\frac{1}{2}} [[\mathbf{v}]]_{i+\frac{1}{2}} \quad (53)$$

where

$$Q_{i+\frac{1}{2}} = \alpha_{i+\frac{1}{2}} \int_{\xi=-1/2}^{1/2} H(v_{i+\frac{1}{2}}(\xi)) d\xi \quad (54)$$

In [56] using comparison, it is shown that flux (50) is entropy stable provided

$$\alpha_{i+\frac{1}{2}} \geq \max_{\lambda, |\xi| \leq 1/2} \left| \lambda \left[A(\mathbf{u}(\mathbf{v}_{i+\frac{1}{2}}(\xi))) \right] \right|. \quad (55)$$

Moreover note that, under (55), inequality $Q_{i+\frac{1}{2}} \geq Q_{i+\frac{1}{2}}^*$ holds. From (51) and (53) we have

$$\mathbf{F}_{i+\frac{1}{2}}^* - \mathbf{F}_{i+\frac{1}{2}} = \frac{1}{2} (Q - Q^*) [[\mathbf{v}]]_{i+\frac{1}{2}}$$

Clearly under condition (55) and from (45), the flux sign stability property (48) holds, therefore the flux (50) is entropy stable. Examples of viscosity coefficient of such entropy stable fluxes are,

- $\alpha_{i+\frac{1}{2}} = \max_{\lambda, |\xi| \leq 1/2} \left| \lambda \left[A(\mathbf{u}(\mathbf{v}_{i+\frac{1}{2}}(\xi))) \right] \right|$ viz Rusanov viscosity [44].
- $\alpha_{i+\frac{1}{2}} = \max_{\lambda, \mathbf{u}} |\lambda [A(\mathbf{u})]|$ viz Lax-Friedrichs viscosity [18].

\square

5.2 High order entropy stable TeCNO flux

The high order numerical fluxes in [1, 11, 16, 36] etc can be written as

$$\mathbf{F}_{i+\frac{1}{2}} = \mathbf{F}_{i+\frac{1}{2}}^* - \frac{1}{2} \tilde{\mathbf{R}}_{i+\frac{1}{2}} \tilde{\mathbf{\Lambda}}_{i+\frac{1}{2}} \langle \langle \tilde{\mathbf{w}} \rangle \rangle_{i+\frac{1}{2}}. \quad (56)$$

Flux (56) is entropy stable provided $\text{sign} \left(\tilde{\mathbf{R}}_{i+\frac{1}{2}}^T \langle \langle \mathbf{v} \rangle \rangle_{i+\frac{1}{2}} \right) = \text{sign} \left(\tilde{\mathbf{R}}_{i+\frac{1}{2}}^T [[\mathbf{v}]]_{i+\frac{1}{2}} \right)$. On using scaled entropy variable relation (21), (56) can be written as

$$\mathbf{F}_{i+\frac{1}{2}}^* - \mathbf{F}_{i+\frac{1}{2}} = \frac{1}{2} \tilde{\mathbf{R}}_{i+\frac{1}{2}} \tilde{\mathbf{\Lambda}}_{i+\frac{1}{2}} \tilde{\mathbf{R}}_{i+\frac{1}{2}}^T \langle \langle \mathbf{v} \rangle \rangle_{i+\frac{1}{2}}, \quad (57)$$

where $\tilde{\mathbf{R}}_{i+\frac{1}{2}} \tilde{\mathbf{\Lambda}}_{i+\frac{1}{2}} \tilde{\mathbf{R}}_{i+\frac{1}{2}}^T \geq 0$ [16]. Thus on using (45), flux sign stability property (48) holds i.e., we have

$$\text{sign} \left(\mathbf{F}_{i+\frac{1}{2}}^* - \mathbf{F}_{i+\frac{1}{2}} \right) = \text{sign} \left(\langle \langle \mathbf{v} \rangle \rangle_{i+\frac{1}{2}} \right) = \text{sign} \left([[\mathbf{u}]]_{i+\frac{1}{2}} \right)$$

□

6 Numerical Result

The approach to construct entropy stable flux (46) is generic and robust as it can work with richly available any entropy conservative \mathbf{F}^* and any non-oscillatory \mathbf{F}^s fluxes. Entropy conservative fluxes for large class of hyperbolic systems can be found in [5, 11, 16, 27, 33, 60] whereas non-oscillatory fluxes can be chosen from [2, 3, 22, 28, 37, 41, 49, 63, 64]. In the following, several numerical tests are presented to demonstrate the accuracy and non-oscillatory capability of entropy stable schemes using various combinations. Precisely, we choose following setting to construct entropy stable non-oscillatory fluxes and obtain the computational results:

Entropy conservative fluxes: We choose entropy conservative flux \mathbf{F}^* given in [33, 54]. In particular, we use the forth order entropy conservative flux

$$\mathbf{F}_{i+\frac{1}{2}}^{*,4} = \frac{4}{3} \mathbf{F}_{i+\frac{1}{2}}^*(\mathbf{u}_i, \mathbf{u}_{i+1}) - \frac{1}{6} (\mathbf{F}_{i+\frac{1}{2}}^*(\mathbf{u}_{i-1}, \mathbf{u}_{i+1}) + \mathbf{F}_{i+\frac{1}{2}}^*(\mathbf{u}_i, \mathbf{u}_{i+2})) \quad (58)$$

and the sixth order entropy conservative flux

$$\begin{aligned} \mathbf{F}_{i+\frac{1}{2}}^{*,6} &= \frac{3}{2} \mathbf{F}_{i+\frac{1}{2}}^*(\mathbf{u}_i, \mathbf{u}_{i+1}) - \frac{3}{10} (\mathbf{F}_{i+\frac{1}{2}}^*(\mathbf{u}_{i-1}, \mathbf{u}_{i+1}) + \mathbf{F}_{i+\frac{1}{2}}^*(\mathbf{u}_i, \mathbf{u}_{i+2})) \\ &\quad + \frac{1}{30} (\mathbf{F}_{i+\frac{1}{2}}^*(\mathbf{u}_{i-2}, \mathbf{u}_{i+1}) + \mathbf{F}_{i+\frac{1}{2}}^*(\mathbf{u}_{i-1}, \mathbf{u}_{i+2}) + \mathbf{F}_{i+\frac{1}{2}}^*(\mathbf{u}_i, \mathbf{u}_{i+3})) \end{aligned} \quad (59)$$

where $\mathbf{F}_{i+\frac{1}{2}}^*(\mathbf{a}, \mathbf{b})$ is second order entropy conservative fluxes satisfying (11) [11, 16, 27, 56, 57].

Non-oscillatory Fluxes: The non-oscillatory fluxes \mathbf{F}^s which we used are first order Local Lax-Friedrichs or Rusanov flux (50), second and third order ENO fluxes [49], third and fifth order WENO-JS fluxes with Jiang-Shu weights [28, 41]. For comparison of results in Figure 3 WENO-Z fluxes with weight [3] is also used. In the m -system case (1), a straightforward and computationally efficient component-wise reconstruction [50] is used as follows:

1. Split the physical flux $\mathbf{f}(\mathbf{u})$ in (1) as,

$$\mathbf{f}(\mathbf{u}) = \mathbf{f}(\mathbf{u})^+ + \mathbf{f}(\mathbf{u})^-, \quad (60)$$

such that $\frac{d\mathbf{f}(\mathbf{u})^+}{d\mathbf{u}} \geq 0$ and $\frac{d\mathbf{f}(\mathbf{u})^-}{d\mathbf{u}} \leq 0$.

2. The m^{th} component of discrete numerical flux $\mathbf{F}_{i+\frac{1}{2}}^\pm$ using ENO/WENO reconstructions is defined as,

$$F_{i+\frac{1}{2}}^{(m)\pm} = v_{i+\frac{1}{2}}^\mp. \quad (61)$$

where $\bar{v}_i = f_i^{(m)\pm}$ is taken as input.

3. Then the non-oscillatory ENO/WENO numerical flux is obtained by,

$$\mathbf{F}_{i+\frac{1}{2}} = \mathbf{F}_{i+\frac{1}{2}}^+ + \mathbf{F}_{i+\frac{1}{2}}^-. \quad (62)$$

Time integration: For time marching in (8), following explicit third order strong stability preserving(SSP) Runge-Kutta methods is used [20, 48].

$$\mathbf{u}^{(1)} = \mathbf{u}^n + \Delta t \mathcal{L}(\mathbf{u}^n), \quad (63)$$

$$\begin{aligned} \mathbf{u}^{(2)} &= \frac{3}{4} \mathbf{u}^{(n)} + \frac{1}{4} \left(\mathbf{u}^{(1)} + \Delta t \mathcal{L}(\mathbf{u}^{(1)}) \right), \\ \mathbf{u}^{(n+1)} &= \frac{1}{3} + \frac{2}{3} \mathbf{u}^{(2)} + \frac{2}{3} \Delta t \mathcal{L}(\mathbf{u}^{(2)}). \end{aligned} \quad (64)$$

where $[\mathcal{L}(\mathbf{u})]_i = -\frac{1}{\Delta x} \left[\left[\hat{\mathbf{F}} \right] \right]_i$.

In order to extend the schemes for multi-dimensional test problems on regular mesh, dimension by dimension or tensorial approach [16, 49] is utilized.

Name Convention: The following name convention is used to annotate the results: legend *EC-m-F^w-n* denotes the numerical result using entropy stable scheme constructed by combination of m^{th} order accurate entropy conservative flux F^* and n^{th} order non-oscillatory flux F^s . For example, EC-6-WENOJS-5 represents entropy stable flux obtained by combining 6^{th} order entropy conservative flux (59) with the fifth order non-oscillatory WENOJS flux [3].

6.1 Scalar conservation law

We consider scalar problems to analyze the accuracy and non-oscillatory nature of various entropy stable schemes obtained by different combinations of entropy conservative fluxes F^* and non-oscillatory fluxes F^s .

6.1.1 Linear transport equation:

Consider the following linear equation

$$u_t + u_x = 0, \quad (65)$$

along with following initial conditions.

- IC1: To test accuracy of schemes:

$$u(x, 0) = -\sin(\pi x), \quad x \in [-1, 1] \quad (66)$$

In Table 1 to 4 the L^∞ and L^1 convergence rate of different non-oscillatory entropy stable schemes is given and compared with the corresponding non-oscillatory scheme with respect to initial condition (66). It can be seen that the entropy stable scheme using m^{th} order entropy conservative flux and n^{th} order non-oscillatory flux *EC-m-F^w-n* maintains the k^{th} order convergence rate where $k = \min(m, n)$.

- IC2: To test non-oscillatory property of schemes:

$$u(x, 0) = \begin{cases} 1 & |x| \leq \frac{1}{10} \\ 0 & \text{else} \end{cases}, \quad x \in [-1, 1] \quad (67)$$

In figures 1, 2 and 3 computed solutions corresponding to initial condition (67) by various entropy stable schemes are given and compared. It can be observed that these entropy stable schemes do not produce any spurious oscillations in the vicinity of discontinuities. From Figures 1 and 2 it can be observed the resolution of discontinuities by entropy stable schemes is characterizes by underlying k^{th} order flux F^* or F^s . In figure 3, results are compared between entropy stable schemes using WENO-JS weights [28] and their modified version improved WENO-Z weights [3] to achieve optimal third-order accuracy regardless of the critical point. This improvement between third order WENO-JS and WENO-Z fluxes also reflects clearly in the computational results in 3 (Left).

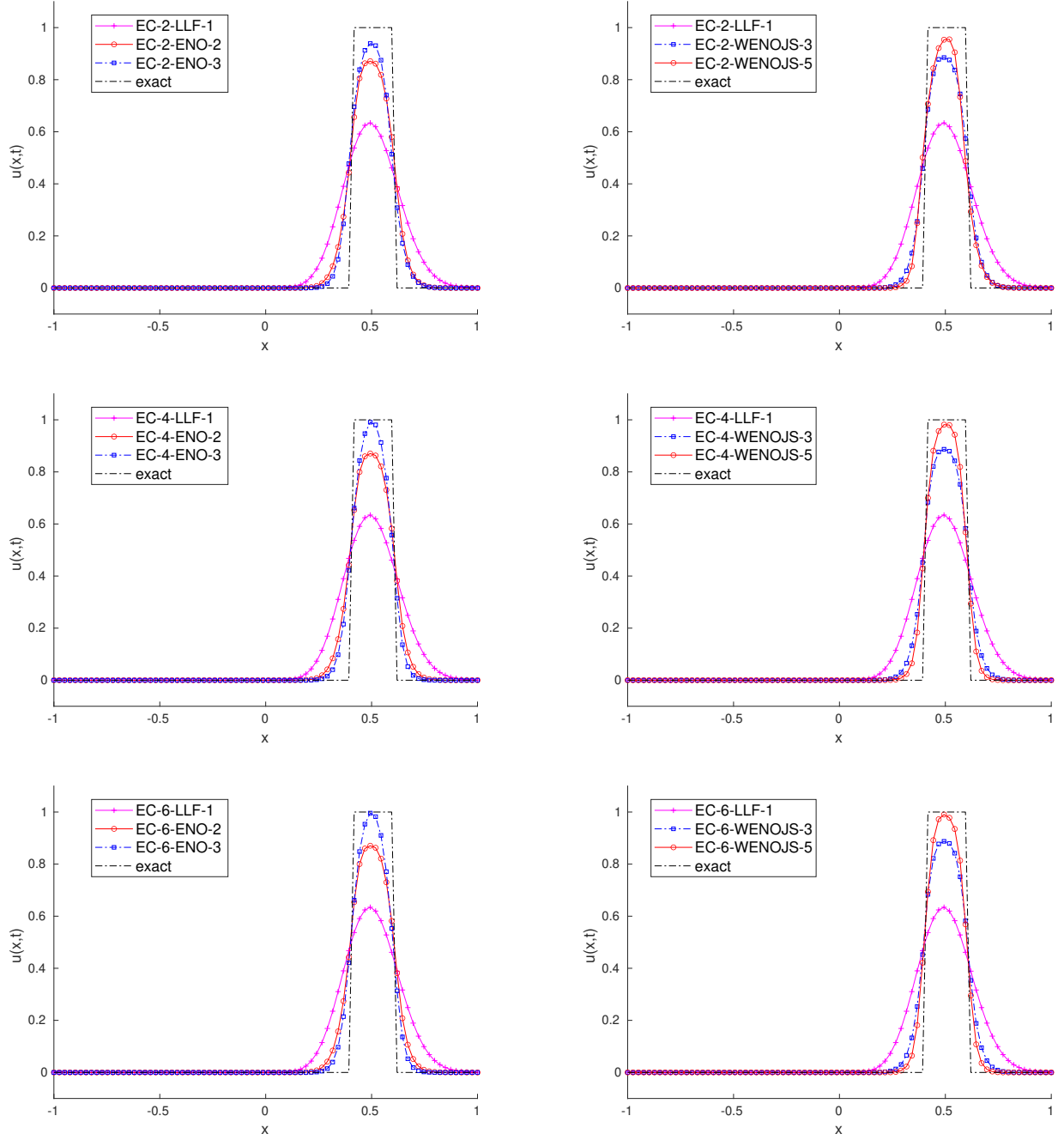


Figure 1: *Linear transport equation for non-oscillatory property:* Each sub figure corresponds to Fixed EC flux F^* with different F^s fluxes.

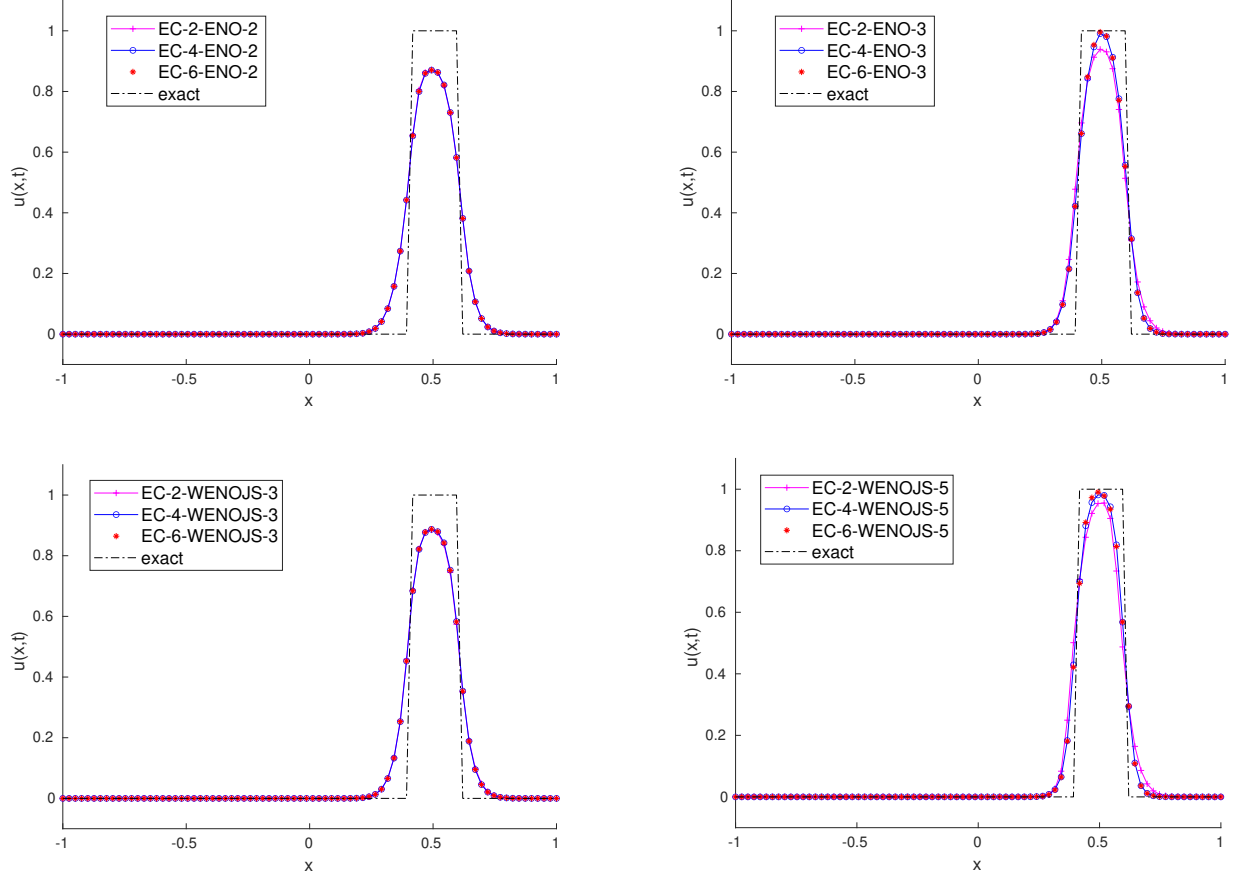


Figure 2: *Linear transport equation for non-oscillatory property*: Each sub figure corresponds to different EC flux with fixed F^s flux

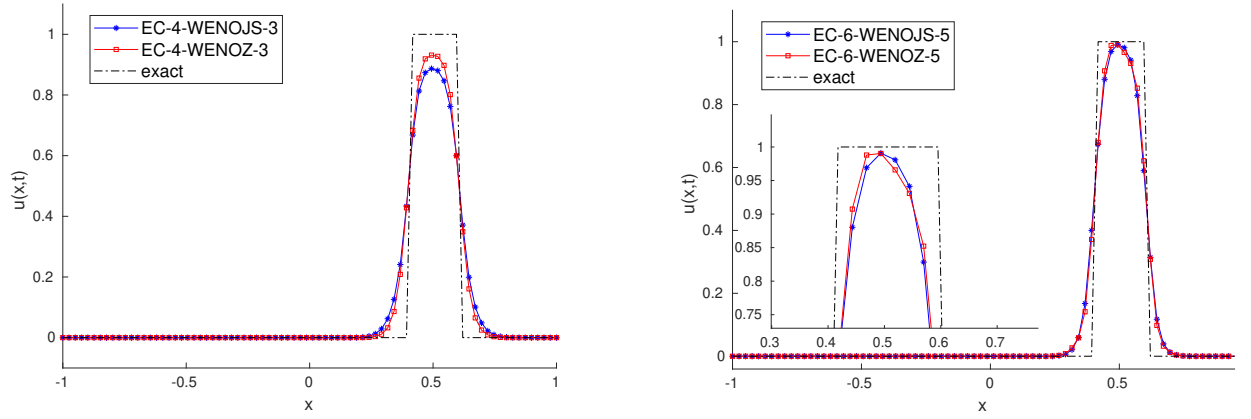


Figure 3: *Linear transport equation for non-oscillatory property*: Different EC fluxes with WENOJS and WENOZ fluxes.

ENO-2

N	L^∞ error	Rate	L^1 error	Rate
20	0.103650350580194	-Inf	0.100929889040078	-Inf
40	0.041704628948130	1.31	0.028772670613416	1.81
80	0.017091991415075	1.29	0.007888602609992	1.87
160	0.006973305119206	1.29	0.002081311252851	1.92
320	0.002825010666346	1.30	0.000547242910005	1.93
640	0.001140808448396	1.31	0.000143102433616	1.94

EC2-ENO-2

20	0.103650350580194	-	0.100929889040078	-
40	0.041704628948130	1.31	0.028772670613416	1.81
80	0.017091991415075	1.29	0.007888602609992	1.87
160	0.006973305119206	1.29	0.002081311252851	1.92
320	0.002825010666346	1.30	0.000547242910005	1.93
640	0.001140808448396	1.31	0.000143102433616	1.94

EC4-ENO-2

20	0.101147595657889	-	0.100570557317309	-
40	0.041672834586009	1.28	0.028450506050033	1.82
80	0.017076078517514	1.29	0.007834801357435	1.86
160	0.006957858965941	1.30	0.002069192494543	1.92
320	0.002822571755367	1.30	0.000544841502157	1.93
640	0.001140309717931	1.31	0.000142661434106	1.93

EC6-ENO-2

20	0.100718064441172	-	0.100246810487900	-
40	0.041640706191883	1.27	0.028443864620176	1.82
80	0.017049582878448	1.29	0.007832290131885	1.86
160	0.006954018562111	1.29	0.002069509727474	1.92
320	0.002821703047318	1.30	0.000544868940700	1.93
640	0.001139926469693	1.31	0.000142666777703	1.93

Table 1: *Linear transport equation*: Convergence rate of base non-oscillatory schemes and corresponding entropy stable schemes $EC-m-F^s-n$ for initial condition (66), $\Delta t = \Delta x^{\frac{5}{3}}$, $Tf = 0.5$

6.1.2 Burgers equation

Consider the Burger's equation

$$u_t + \left(\frac{u^2}{2} \right)_x = 0, \quad x \in [-1, 1] \quad (68)$$

with periodic boundary condition. The following initial conditions are chosen

- IC3: To test accuracy of schemes:

$$u(x, 0) = 1 + \frac{1}{2} \sin(\pi x), \quad (69)$$

The solution of Burgers equation corresponding to (69) remains smooth until pre-shock time $T = Tb$. In Table 6.1.2, the L^∞ and L^1 convergence rate of different non-oscillatory entropy stable schemes is given and compared with the corresponding non-oscillatory scheme with respect to initial condition (66). Similar to linear case, entropy stable schemes $EC-m-F^w-n$ maintains the k^{th} order convergence rate where $k = \min(m, n)$.

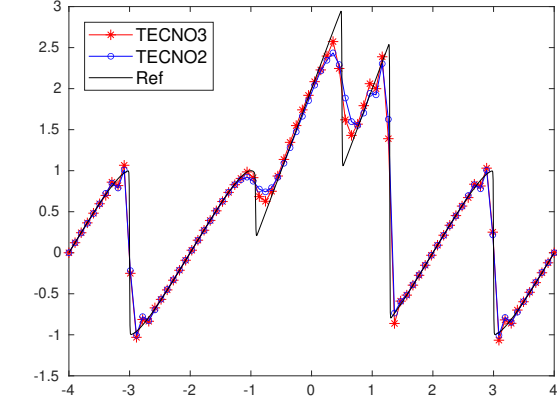
ENO-3				
20	0.005406480964691	-	0.006734873704422	-
40	0.000616301811662	3.13	0.000730929733999	3.20
80	0.000072520785343	3.09	0.000085989470177	3.09
160	0.000008791230376	3.04	0.000010393579292	3.05
320	0.000001077164992	3.03	0.000001280407541	3.02
640	0.000000132451830	3.02	0.000000158874708	3.01
EC2-ENO-3				
20	0.050543475632165	-	0.047520338901013	-
40	0.021966858587848	1.20	0.013346936006220	1.83
80	0.009471535241998	1.21	0.003601408089964	1.89
160	0.003984836829451	1.25	0.000973727113086	1.89
320	0.001653962671563	1.27	0.000259703997357	1.91
640	0.000674588416101	1.29	0.000068309161723	1.93
EC4-ENO-3				
20	0.005547400761271	-	0.006753254108990	-
40	0.000631519872228	3.13	0.000731575516321	3.21
80	0.000074491329863	3.08	0.000086022367170	3.09
160	0.000009045052137	3.04	0.000010395657689	3.05
320	0.000001113643600	3.02	0.000001280564509	3.02
640	0.000000137250298	3.02	0.000000158885516	3.01
EC6-ENO-3				
20	0.007039299255173	-	0.008204945851443	-
40	0.000863983047168	3.03	0.000970359664068	3.08
80	0.000094006201842	3.20	0.000108905524817	3.16
160	0.000011206410794	3.07	0.000013134852567	3.05
320	0.000001354597352	3.05	0.000001612869148	3.03
640	0.000000165232131	3.04	0.000000199829737	3.01

Table 2: *Linear transport equation case*: Convergence rate of non-oscillatory schemes and corresponding entropy stable schemes $EC-m-F^s-n$, for initial condition (66), $\Delta t = \Delta x^{\frac{5}{3}}$, $Tf = 0.5$

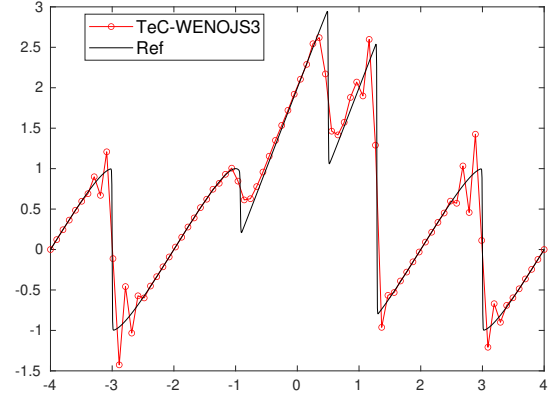
- IC4: To test non-oscillatory property:

$$u(x, 0) = \begin{cases} \sin(\pi x) & |x| > 4 \\ 3 & -1 \leq x \leq -0.5 \\ 1.0 & -0.5 \leq x \leq 0 \\ 3.0 & 0.0 \leq x < 0.5 \\ 1.0 & \text{else.} \end{cases} \quad x \in [-4, 4] \quad (70)$$

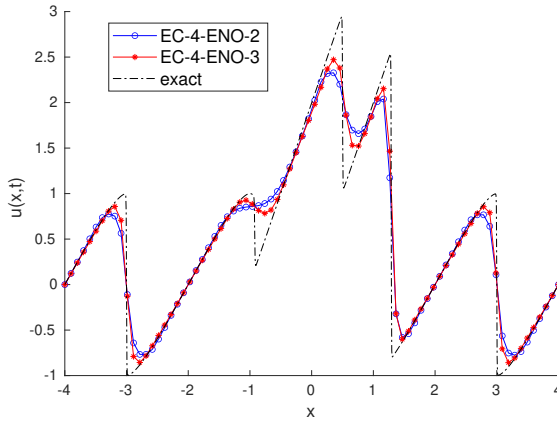
The initial condition (70) contains smooth and discontinuous data regions which eventually develops a complex solution containing stationary shock at $x = \pm 3$, rarefaction waves and moving shocks of varied intensities. In Figure 4, numerical solution computed by different high order entropy stable schemes is given compared. It can be observed from results in sub-figures 4(a) and 4(b) that entropy stable non-oscillatory *TeCNO* schemes proposed in [16] and low dissipative *TeC-WENOJS3* scheme in [1] respectively exhibits oscillations at discontinuities. However, the proposed entropy stable schemes $EC-m-F^w-n$ in this work give non-oscillatory solution as shown in sub-figures 4(c) and 4(d). Moreover, the resolution of discontinuities is characterized by the base non-oscillatory flux used in the construction of entropy stable scheme.



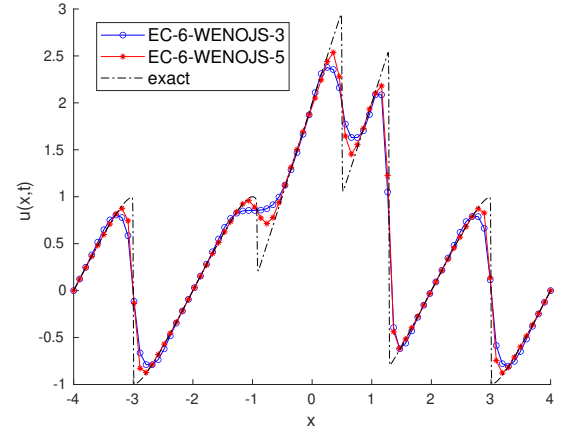
(a)



(b)



(c)



(d)

Figure 4: Non-oscillatory solution of Burgers equation by $EC-m-F^n$ schemes corresponding to (70) at $T = 0.5$, $CFL = 0.8$, $N = 80$. Small spurious oscillations can be observed TECNO [16] and TeC-WENOJS3 [1] schemes.

WENOJS-3

20	0.095295719529242	-	0.097589964487292	-
40	0.037882127968846	1.33	0.024549404055603	1.99
80	0.014499096466708	1.39	0.005929934948099	2.05
160	0.004486646249450	1.69	0.001166681092555	2.35
320	0.000792775926365	2.50	0.000138843470203	3.07
640	0.000050791668167	3.96	0.000013117165987	3.40

EC2-WENOJS-3

20	0.096619636409225	-	0.096363607474423	-
40	0.038750928270435	1.32	0.025351032277798	1.93
80	0.014977670426086	1.37	0.006266304072526	2.02
160	0.004879825577255	1.62	0.001327973739958	2.24
320	0.001273255037385	1.94	0.000226978005982	2.55
640	0.000361908965099	1.81	0.000042452734679	2.42

EC4-WENOJS-3

20	0.093949645707552	-	0.096603590083196	-
40	0.037699524785342	1.32	0.024559646487770	1.98
80	0.014450852094813	1.38	0.005857712856211	2.07
160	0.004461105840692	1.70	0.001117876971273	2.39
320	0.000823176706129	2.44	0.000122547918652	3.19
640	0.000170130196615	2.27	0.000012785439939	3.26

EC6-WENOJS-3

20	0.006091950556727	-Inf	0.006795899050582	-Inf
40	0.000693581835622	3.13	0.000733637225341	3.21
80	0.000080943147491	3.10	0.000086141984941	3.09
160	0.000009655813762	3.07	0.000010401032181	3.05
320	0.000001168287450	3.05	0.000001280810577	3.02
640	0.000000141575726	3.04	0.000000158895341	3.01

Table 3: *Linear transport equation*: Convergence rate of non-oscillatory schemes and corresponding entropy stable schemes $EC-m-F^s-n$, for initial condition (66), $CFL = 0.8$, $\Delta t = \Delta x^{\frac{5}{3}}$, $Tf = 0.5$

6.2 Systems of Conservation Laws

Like scalar case, in system case also various proposed entropy stable schemes $EC-m-F^w-n$ are used to compute the numerical solution of hyperbolic systems. However to restrict the length of the presentation, in one dimensional tests, results are reported only for third and fifth order entropy stable $ES-4-ENO-3$ and $ES-6-WENOJS-5$ schemes. Also results are compared with results by base non-oscillatory $ENO-3$ and $WENOJS-5$ schemes respectively. In two dimensional test cases, computational results by fifth order non-oscillatory entropy stable scheme $EC6-WENOJS-5$ are given and compared with results of non-oscillatory WENO scheme $WENOJS-5$.

6.2.1 The 1D Euler system

The one dimensional system of Euler equations is given by

$$\begin{pmatrix} \rho \\ \rho u \\ E \end{pmatrix}_t + \begin{pmatrix} \rho u \\ \rho u^2 + p \\ u(E + p) \end{pmatrix}_x = 0, \quad (71)$$

where following relationship holds between density (ρ), pressure(p) and energy(E)

$$p = (\gamma - 1) \left(E - \frac{1}{2} \rho u^2 \right). \quad (72a)$$

WENOJS-5

N	L^∞ error	Rate	L^1 error	Rate
20	0.001063307461522	-	0.001067470709297	-
40	0.000028857556769	5.20	0.000027413329345	5.28
80	0.000000838767067	5.10	0.000000777342539	5.14
160	0.000000024195642	5.12	0.000000023316656	5.06
320	0.000000000666380	5.18	0.000000000716246	5.02
640	0.000000000019484	5.10	0.000000000022600	4.99

EC4-WENOJS-5

20	0.000902851352136	-	0.001054980033863	-
40	0.000105655879544	3.10	0.000056640425063	4.22
80	0.000011827762287	3.16	0.000003516274955	4.01
160	0.000001314715704	3.17	0.000000228819055	3.94
320	0.000000144469908	3.19	0.000000014882411	3.94
640	0.000000015851658	3.19	0.000000000964265	3.95

EC6-WENOJS-5

20	0.000981495800376	-	0.001013770549779	-
40	0.000027221380075	5.17	0.000026652053956	5.25
80	0.000000808887363	5.07	0.000000774174265	5.11
160	0.000000023875431	5.08	0.000000023322080	5.05
320	0.000000000666377	5.16	0.000000000716247	5.03
640	0.000000000019488	5.10	0.000000000022600	4.99

Table 4: *Linear transport equation*: Convergence rate of non-oscillatory schemes and corresponding entropy stable schemes $EC-m-F^s$ - n , $m > n$, for initial condition (66), $CFL = 0.8$, $\Delta t = \Delta x^{\frac{5}{3}}$, $Tf = 0.5$

where γ is the ratio of specific heat coefficient. Computational results are obtained for various Riemann problem of the form [59]

$$u(x, 0) = \begin{cases} u_l & \text{if } x < x_0 \\ u_r & \text{if } x \geq x_0 \end{cases} \quad (73a)$$

where $u_l = (\rho_l, u_l, p_l)$ and $u_r = (\rho_r, u_r, p_r)$.

Sod shock tube test:

The sod problem is defined in [52] is given by following initial condition

$$u(x, 0) = \begin{cases} (1, 0, 1) & \text{if } -5 < x < 0 \\ (0.125, 0, 0.1) & \text{if } 0 \leq x \leq 5 \end{cases} \quad (74a)$$

for this initial condition the evolved solution consists of a rarefaction wave followed by a contact discontinuity and the shock discontinuity. The numerical solution for this test is given in Figure 5.

ENO-3

20	0.004089806180465	-Inf	0.002576711084414	-Inf
40	0.000652957611008	2.65	0.000330110340694	2.96
80	0.000135597656038	2.27	0.000044560530326	2.89
160	0.000029932048665	2.18	0.000006236888973	2.84
320	0.000006346061054	2.24	0.000000951369850	2.71

EC4-ENO-3

20	0.003984058473352	-Inf	0.002564119225979	-Inf
40	0.000697102270904	2.51	0.000332755325627	2.95
80	0.000141257762097	2.30	0.000044795195031	2.89
160	0.000030229316719	2.22	0.000006251616266	2.84
320	0.000006352967047	2.25	0.000000953700271	2.71

WENOJS-3

20	0.030054283683825	-Inf	0.021503606487366	-Inf
40	0.011645863708584	1.37	0.005705413057081	1.91
80	0.004446629544148	1.39	0.001272279921921	2.16
160	0.001229792324948	1.85	0.000209695528475	2.60
320	0.000160195787758	2.94	0.000019563728701	3.42

EC4-WENOJS-3

20	0.028159747571163	-Inf	0.021200069278609	-Inf
40	0.011420125749124	1.30	0.005621069554234	1.92
80	0.004354218766912	1.39	0.001256133850256	2.16
160	0.001195708298807	1.86	0.000201484286229	2.64
320	0.000180158182566	2.73	0.000016295119155	3.63

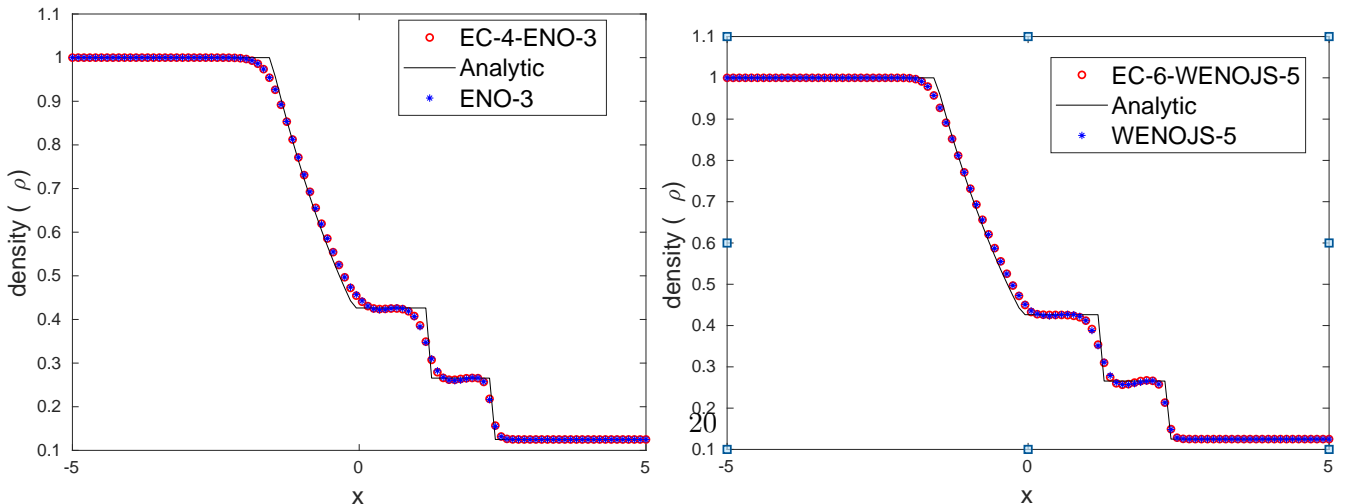
WENOJS-5

N	L^∞ error	Rate	L^1 error	Rate
20	0.001585602535748	-Inf	0.000868966169066	-Inf
40	0.000040536940062	5.29	0.000025150570223	5.11
80	0.000001917646443	4.40	0.000000750072987	5.07
160	0.000000150942973	3.67	0.000000023675030	4.99
320	0.000000003900132	5.27	0.000000000587218	5.33

EC6-WENOJS-5

20	0.001503755255236	-Inf	0.000839061370388	-Inf
40	0.000040903613295	5.20	0.000024422796621	5.10
80	0.000001973978420	4.37	0.000000736081852	5.05
160	0.000000153479630	3.68	0.000000023303174	4.98
320	0.000000004094550	5.23	0.000000000572338	5.35

Table 5: *Burgers equation*: Convergence rate of base non-oscillatory schemes and corresponding entropy stable schemes for initial condition (69), $CFL = 0.4$, $\Delta t = \Delta x^{\frac{5}{3}}$, $Tf = \frac{1}{2\pi}$



Laney Shock tube Test

A more complicated shock tube test problem to check the non-oscillatory property of any numerical scheme is governed by the initial Riemann data

$$u(x, 0) = \begin{cases} (1.0, 0, 100000) & \text{if } x < 0 \\ (0.01, 0, 1000) & \text{if } 0 \leq x \leq 0 \end{cases} \quad (75a)$$

In this test, the ratio of left and right states of density and pressure across initial discontinuity is very high and right initial state of density is close to zero. Therefore, computationally, even small oscillations can lead to negative density or pressure, which results into nonphysical imaginary speed of sound $c = \sqrt{\frac{\gamma p}{\rho}}$. The numerical solution for this test case is given in Figure 6.

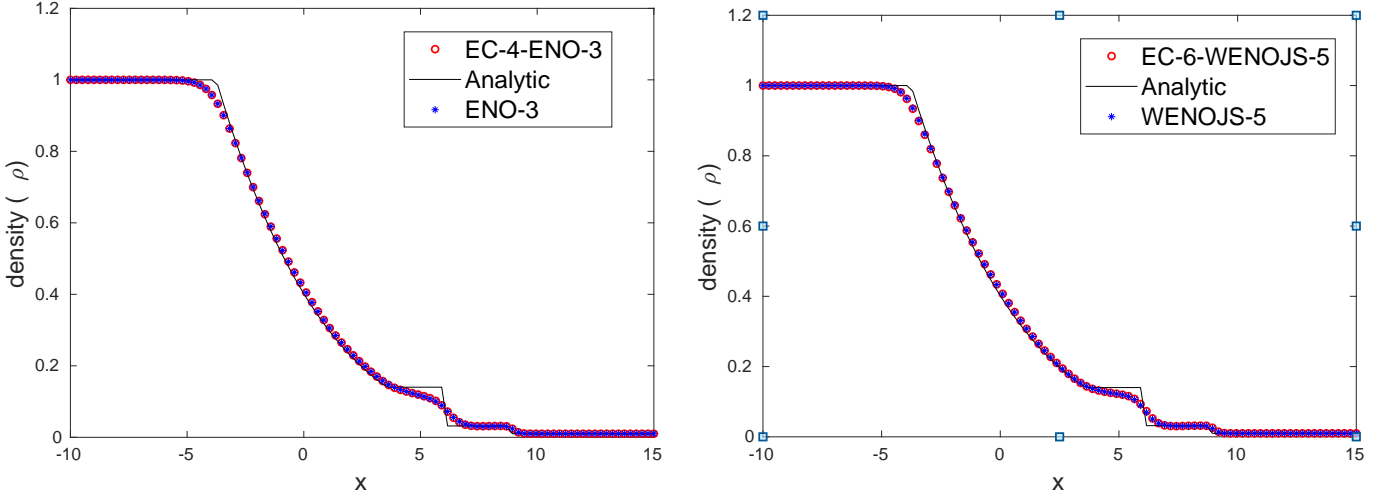


Figure 6: Density plot for Laney test with $N = 100, CFL = 0.25, T = 0.01$

Lax tube test:

We consider the Lax tube problem discussed in [32] with the initial condition given by

$$u(x, 0) = \begin{cases} (0.445, 0.698, 3.528) & \text{if } -5 < x < 0 \\ (0.5, 0, 0.571) & \text{if } 0 \leq x \leq 5 \end{cases} \quad (76a)$$

solution corresponding this initial condition contains a right traveling strong shock wave, a contact surface, and a left rarefaction wave. The numerical solution for this test case is given in Figure 7.

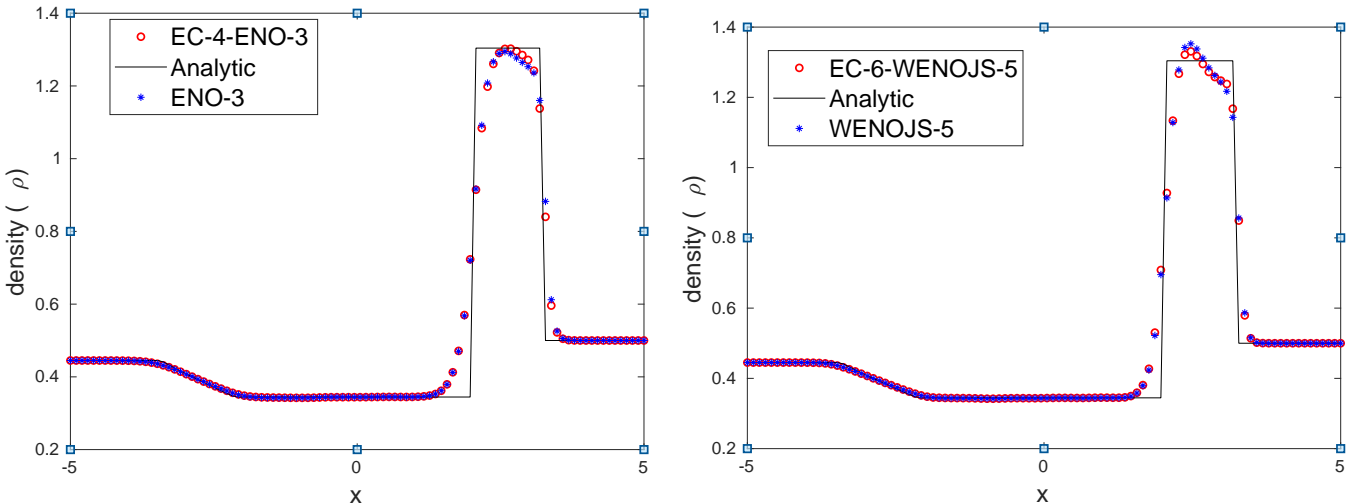


Figure 7: Solution at $N = 100, CFL = 0.25, T = 1.3$

Shock-entropy wave interaction

[51] This Shu-Osher problem is govern by following initial condition

$$u(x, 0) = \begin{cases} (3.857143, 2.629369, 2.629369) & \text{if } -5 < x < 0 \\ (1 + \epsilon \sin(kx), 0, 1) & \text{if } 0 \leq x \leq 5 \end{cases} \quad \epsilon = 0.2, k = 5, \quad (77a)$$

which simulates shock-turbulence interaction in which a strong shock wave propagates into density filed with artificial fluctuations with amplitude $\epsilon =$ and wave number k . This problem tests the capability of any scheme to accurately capture a shock wave, its interaction with an unsteady density field, and the sinusoidal waves propagating downstream of the shock. The numerical solution for this test case is given in Figure 8.

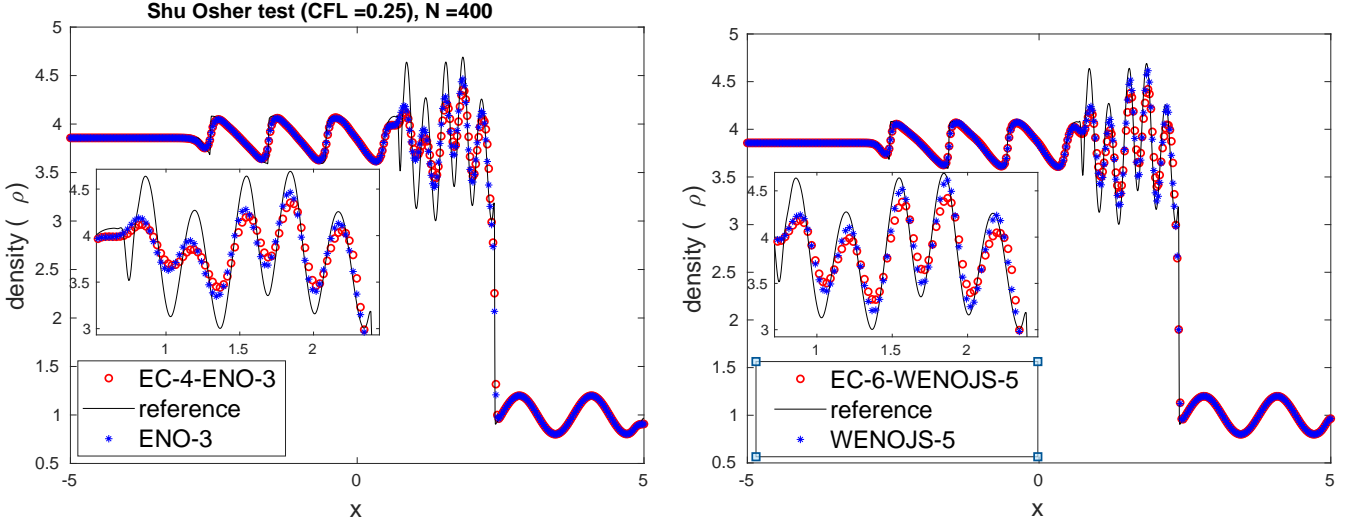


Figure 8: Density plot for Shu-Osher test with $N = 400, CFL = 0.25, T = 1.8$.

Two interacting blast wave

Wood-Colella blast wave [61] is another interesting problem to test the shock capturing ability of numerical scheme given by following initial condition

$$u(x, 0) = \begin{cases} (1.0, 0.0, 1000.0) & \text{if } 0.0 < x < 0.1 \\ (1.0, 0.0, 0.01) & \text{if } 0.1 \leq x \leq 0.9 \\ (1.0, 0.0, 100.0) & \text{if } 0.9 \leq x \leq 1.0. \end{cases} \quad (78a)$$

This problem involves the multiple interactions of shock, contact, and rarefaction wave. A reflecting boundary condition is applied at the boundary of the domain $x = 0$ and $x = 1$. The numerical solution for this test case is given in Figure 9.

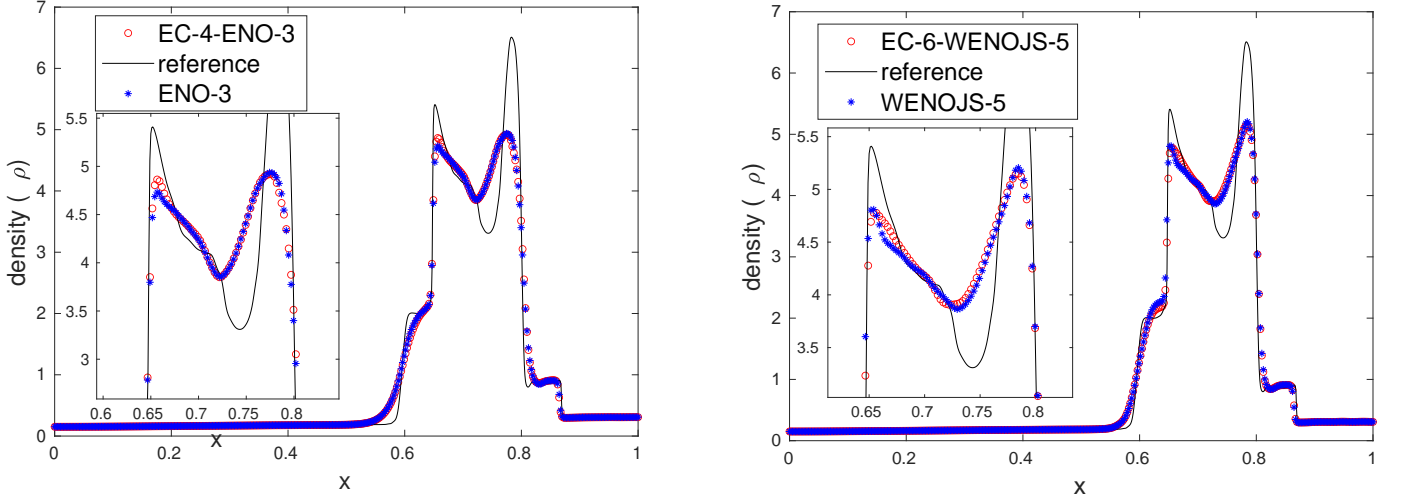


Figure 9: Density plot for two interacting blast wave test $N = 400, CFL = 0.25, T = 0.038$

From figures 5 and 6 for Sod and Laney shock tube test respectively show that solution by entropy stable schemes is almost identical with that of solution by shock capturing non-oscillatory ENO/WENO schemes. The comparison of the approximated solution by entropy stable schemes and ENO/WENO schemes is clearly visible in figures 7-9. It can be concluded from numerical results for 1D shock tube problems in figures 5-9, that high order entropy stable schemes $EC-4-ENO-3$ and $EC-6-WENOJS-5$ yield non-oscillatory solutions even for complex flow and results are comparable with ENO/WENO schemes.

6.3 2D Euler equation

In this section the proposed scheme is applied to 2D Euler equations

$$\begin{pmatrix} \rho \\ \rho u \\ \rho v \\ E \end{pmatrix}_t + \begin{pmatrix} \rho u \\ \rho u^2 + p \\ \rho uv \\ u(E + p) \end{pmatrix}_x + \begin{pmatrix} \rho v \\ \rho uv \\ \rho v^2 + p \\ v(E + p) \end{pmatrix}_y = 0. \quad (79)$$

where ρ is density and u, v are component of velocity along x and y direction respectively. The pressure and energy are related by following

$$E = \frac{p}{\gamma - 1} + \frac{\rho(u^2 + v^2)}{2} \quad (80a)$$

and γ is the ratio of specific heat. The following test problems are considered for testing the performance of the scheme for equation (79). In all the tests numerical solution using fifth order non-oscillatory entropy stable scheme $EC6-WENOJS-5$ is compared with the base non-oscillatory schemes $WENOJS-5$. Solution plots are given in figure side by side

2D Riemann problem [31, 46] Consider 2D Euler equations (79) with Riemann data defined in in following way,

$$(p, \rho, u, v) = \begin{cases} (1.5000, 1.5000, 0.0000, 0.0000) & \text{if } x > 0.5 \text{ and } y > 0.5, \\ (0.3000, 0.5323, 1.2060, 0.0000) & \text{if } x < 0.9 \text{ and } y \geq 0.5, \\ (0.0290, 0.1380, 1.2060, 1.2060) & \text{if } x < 0.5 \text{ and } y < 0.5, \\ (0.3000, 0.5323, 0.0000, 1.2060) & \text{if } x > 0.5 \text{ and } y < 0.5. \end{cases} \quad (81)$$

Solution for this initial condition is computed at time $t = 0.5$ and corresponding filled contour plots are given in figure 10.

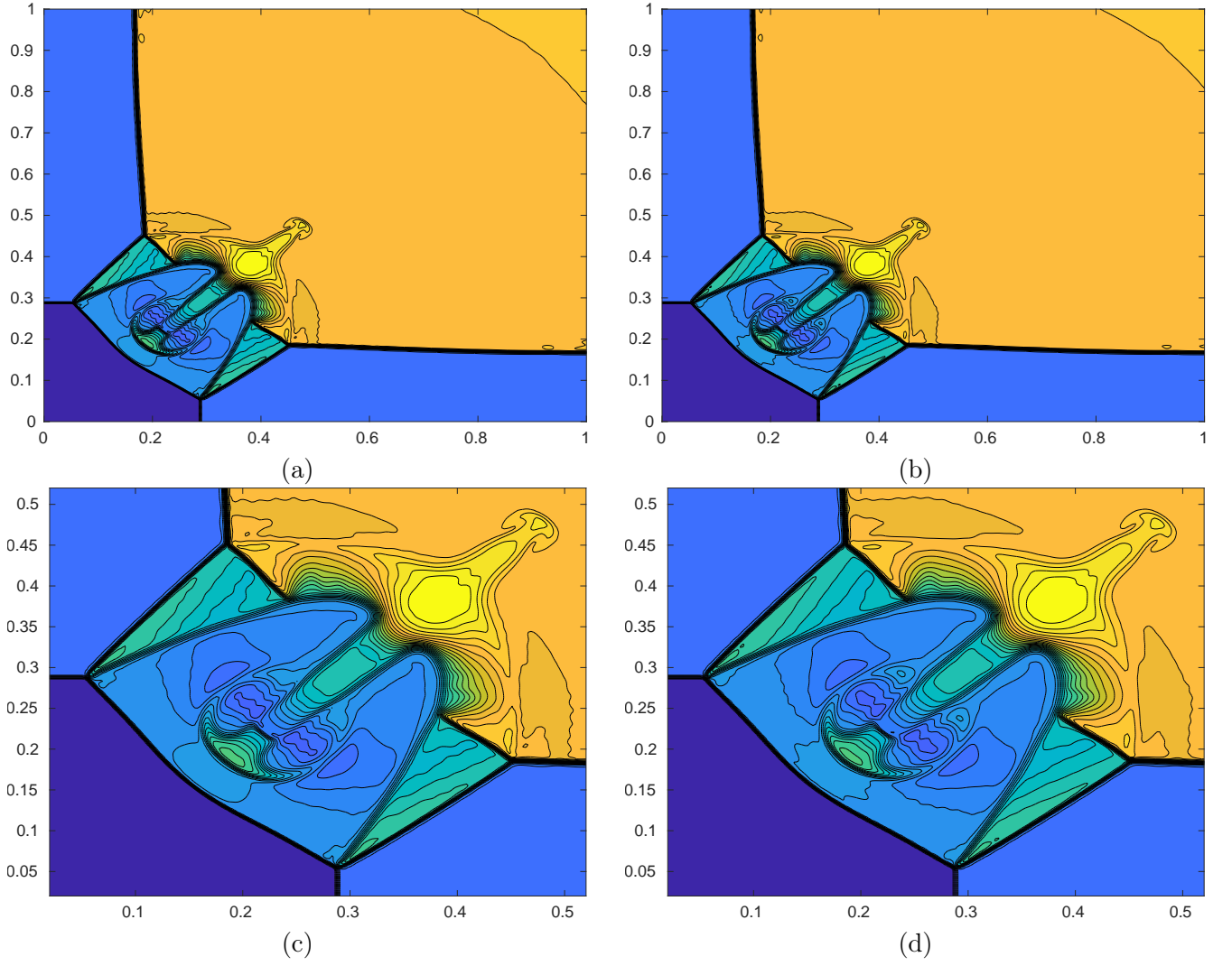


Figure 10: Contour solution plot of 2D Riemann problem with 31 of contour lines corresponding to configuration (81). Solution by *WENOJS-5* is in (a) and zoomed version in (c). Solution by *EC6-WENOJS-5* is in (b) and zoomed version in (d)., $CFL = 0.25$, $t = 0.5$, $N = 400 \times 400$

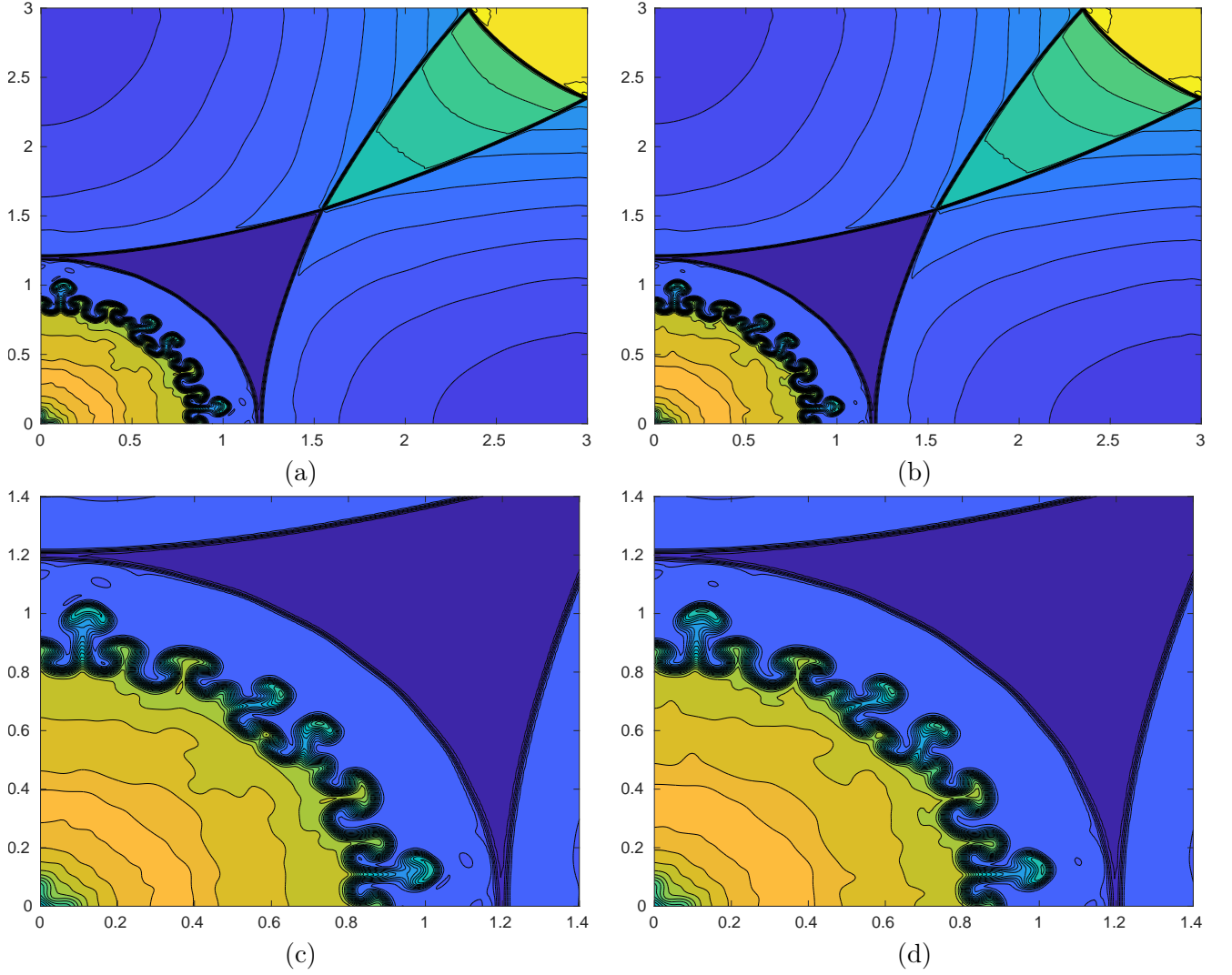


Figure 11: Contour solution plot of 2D Riemann problem with 31 of contour lines corresponding to explosion problem (82). Solution by *WENOJS-5* is in (a) and zoomed version in (c). Solution by *EC6-WENOJS-5* is in (b) and zoomed version in (d)., $CFL = 0.45$, $t = 3.2$, $N = 400 \times 400$

Explosion problem [35] The explosion test problem is setup in a square domain $[-3, 3] \times [-3, 3]$ in x - y plane. The initial Riemann data is separated in the domain by a circle with center $(0, 0)$ and radius 0.4. The initial density and pressure are defined in following way.

$$\begin{cases} \rho(x, y) = 1, p(x, y) = 1, & \text{if } x^2 + y^2 < (0.4)^2 \\ \rho(x, y) = 0.125, p(x, y) = 0.1. & \text{otherwise} \end{cases} \quad (82a)$$

The filled contour plot of numerical results for explosion problem are shown and compared in figure 11.

Implosion [26] Consider the implosion problem modeled inside a square domain $[-0.3, 0.3] \times [-0.3, 0.3]$ in $x - y$ plane. Initial Density and pressure distribution of the gas are following,

$$\begin{cases} \rho(x, y) = 0.125, p(x, y) = 0.14, & \text{if } |x| + |y| < 0.15 \\ \rho(x, y) = 1, p(x, y) = 1. & \text{otherwise} \end{cases}$$

Initially the velocities are kept zero in the computational domain $[0, 0.3] \times [0, 0.3]$ with reflecting boundary. Computation is done only for upper right quadrant $(x, y) \in (0, 0.3) \times (0, 0.3)$ as in [2, 35]. The numerical results are shown and compared in Figure 12.

$$\begin{cases} \rho(x, y) = 1, p(x, y) = 1, & \text{if } x^2 + y^2 < (0.4)^2 \\ \rho(x, y) = 0.125, p(x, y) = 0.1. & \text{otherwise} \end{cases} \quad (83a)$$

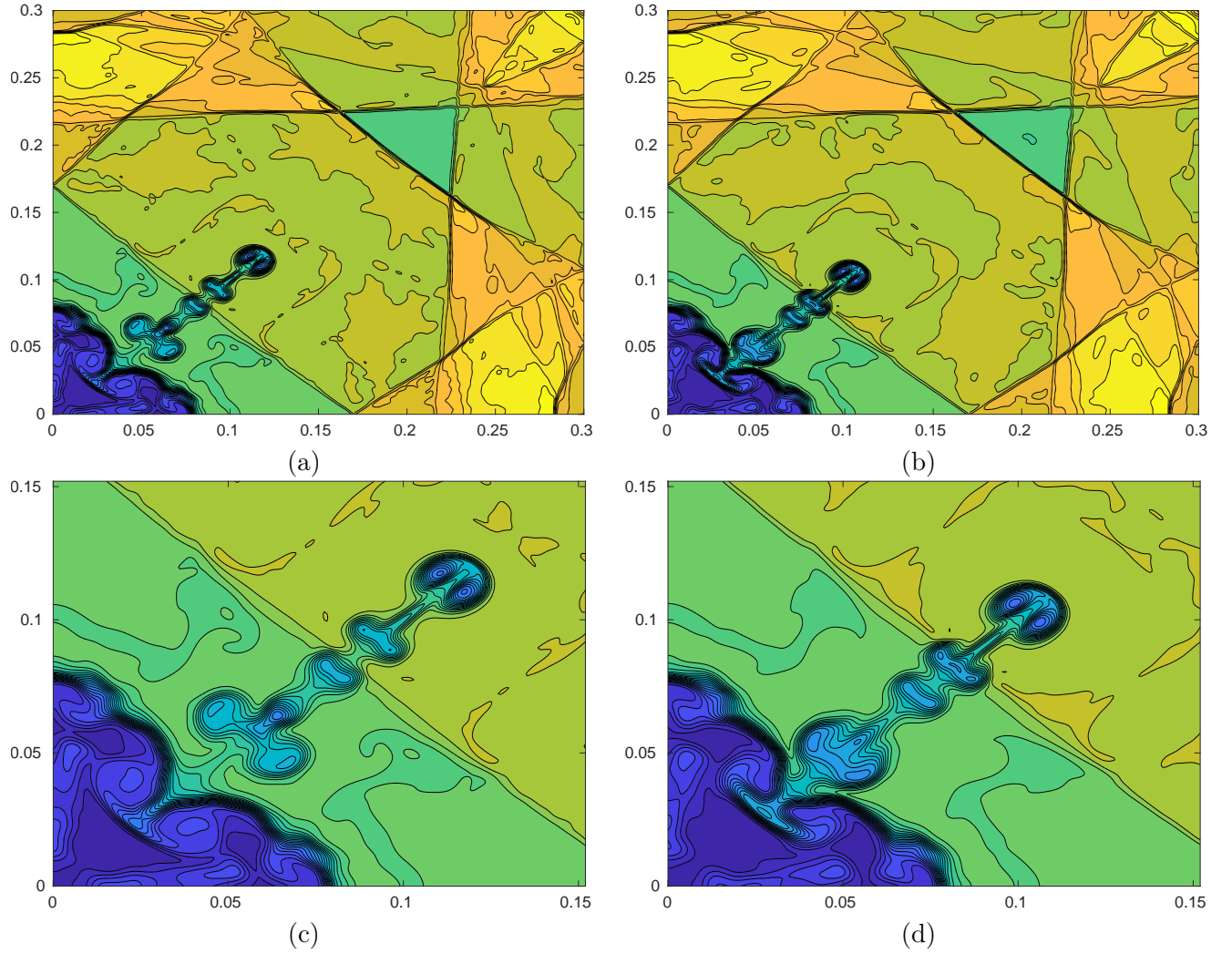


Figure 12: Contour solution plot of 2D Riemann problem with 31 of contour lines corresponding to implosion problem (83). Solution by *WENOJS-5* is in (a) and zoomed version in (c). Solution by *EC6-WENOJS-5* is in (b) and zoomed version in (d)., $CFL = 0.45$, $t = 3.2$, $N = 400 \times 400$

From the numerical results for 2D Euler tests in figures 10-12 it is clear *EC6-WENOJS-5* captures feature of the flow and results are comparable to WENO5JS scheme.

7 Conclusion

In this work, problem of constructing non-oscillatory arbitrary order entropy stable flux is solved by framing it as least square optimization problem. Based on optimization, entropy stable flux is proposed which utilizes a *flux sign stability property*. Some of the existing entropy stable fluxes are retrospectively shown to satisfy the flux sign stability property. The proposed approach is robust and works well with any entropy conservative and non-oscillatory flux. Numerical results also established that such constructed entropy stable schemes give excellent non-oscillatory results even for complex problems. Moreover for smooth solution region these schemes retains formal order of accuracy of lower order flux used in the construction.

References

- [1] BISWAS, B., AND DUBEY, R. K. Low dissipative entropy stable schemes using third order weno and tvd reconstructions. *Advances in Computational Mathematics* (Dec 2017).
- [2] BISWAS, B., AND DUBEY, R. K. Eno and weno schemes using arc-length based smoothness measurement. *Computers & Mathematics with Applications* 80, 12 (2020), 2780–2795.
- [3] BORGES, R., CARMONA, M., COSTA, B., AND DON, W. S. An improved weighted essentially non-oscillatory scheme for hyperbolic conservation laws. *Journal of Computational Physics* 227, 6 (2008), 3191–3211.
- [4] CASTRO, M., COSTA, B., AND DON, W. S. High order weighted essentially non-oscillatory weno-z schemes for hyperbolic conservation laws. *Journal of Computational Physics* 230, 5 (2011), 1766–1792.
- [5] CHANDRASHEKAR, P. Kinetic energy preserving and entropy stable finite volume schemes for compressible euler and navier-stokes equations. *Communications in Computational Physics* 14, 05 (nov 2013), 1252–1286.
- [6] CHEN, R., AND MAO, D.-K. Entropy-tvd scheme for nonlinear scalar conservation laws. *Journal of Scientific Computing* 47, 2 (2011), 150–169.
- [7] CHEN, R., ZOU, M., AND XIAO, L. Entropy-tvd scheme for the shallow water equations in one dimension. *Journal of Scientific Computing* 71, 2 (2017), 822–838.
- [8] CHENG, X. A fourth order entropy stable scheme for hyperbolic conservation laws. *Entropy* 21, 5 (2019).
- [9] CHENG, X., AND NIE, Y. A third-order entropy stable scheme for hyperbolic conservation laws. *Journal of Hyperbolic Differential Equations* 13, 01 (2016), 129–145.
- [10] CRANDALL, M., MAJDA, A., AND CENTER., W. U.-M. M. R. *Monotone Difference Approximations for Scalar Conservation Laws*. MRC technical summary report. Mathematics Research Center, University of Wisconsin, 1979.
- [11] DUAN, J., AND TANG, H. High-order accurate entropy stable finite difference schemes for the shallow water magnetohydrodynamics. *Journal of Computational Physics* 431 (2021), 110136.
- [12] DUBEY, R. K., AND BISWAS, B. Suitable diffusion for constructing non-oscillatory entropy stable schemes. *Journal of Computational Physics* (2018).
- [13] EVANS, L. *Partial Differential Equations*. Graduate studies in mathematics. American Mathematical Society, 1998.

- [14] FAN, P., SHEN, Y., TIAN, B., AND YANG, C. A new smoothness indicator for improving the weighted essentially non-oscillatory scheme. *Journal of Computational Physics* 269 (2014), 329–354.
- [15] FISHER, T. C., AND CARPENTER, M. H. High-order entropy stable finite difference schemes for nonlinear conservation laws: Finite domains. *Journal of Computational Physics* 252 (2013), 518 – 557.
- [16] FJORDHOLM, U. S., MISHRA, S., AND TADMOR, E. Arbitrarily high-order accurate entropy stable essentially nonoscillatory schemes for systems of conservation laws. *SIAM Journal on Numerical Analysis* 50, 2 (jan 2012), 544–573.
- [17] FJORDHOLM, U. S., MISHRA, S., AND TADMOR, E. Eno reconstruction and eno interpolation are stable. *Foundations of Computational Mathematics* 13, 2 (apr 2013), 139–159.
- [18] FRIEDRICHS, K. O. Symmetric hyperbolic linear differential equations. *Communications on Pure and Applied Mathematics* 7, 2 (1954), 345–392.
- [19] GOODMAN, J. B., AND LEVEQUE, R. J. A geometric approach to high resolution tvd schemes. *SIAM Journal on Numerical Analysis* 25, 2 (1988), 268–284.
- [20] GOTTLIEB, S., AND SHU, C.-W. Total variation diminishing runge-kutta schemes. *Math. Comput.* 67, 221 (Jan. 1998), 73–85.
- [21] HA, Y., KIM, C. H., LEE, Y. J., AND YOON, J. An improved weighted essentially non-oscillatory scheme with a new smoothness indicator. *Journal of Computational Physics* 232, 1 (2013), 68–86.
- [22] HARTEN, A. High resolution schemes for hyperbolic conservation laws. *Journal of Computational Physics* 49, 3 (1983), 357 – 393.
- [23] HARTEN, A., AND LAX, P. D. On a class of high resolution total-variation-stable finite-difference schemes. *SIAM Journal on Numerical Analysis* 21, 1 (1984), pp. 1–23.
- [24] HARTEN, A., AND OSHER, S. Uniformly high-order accurate nonoscillatory schemes. i. *SIAM Journal on Numerical Analysis* 24, 2 (1987), 279–309.
- [25] HENRICK, A. K., ASLAM, T. D., AND POWERS, J. M. Mapped weighted essentially non-oscillatory schemes: achieving optimal order near critical points. *Journal of Computational Physics* 207, 2 (2005), 542–567.
- [26] HUI, W., LI, P., AND LI, Z. A unified coordinate system for solving the two-dimensional euler equations. *Journal of Computational Physics* 153, 2 (1999), 596 – 637.
- [27] ISMAIL, F., AND ROE, P. L. Affordable, entropy-consistent euler flux functions ii: Entropy production at shocks. *Journal of Computational Physics* 228, 15 (aug 2009), 5410–5436.
- [28] JIANG, G.-S., AND SHU, C.-W. Efficient implementation of weighted eno schemes. *Journal of computational physics* 126, 1 (1996), 202–228.
- [29] KIM, C. H., HA, Y., AND YOON, J. Modified non-linear weights for fifth-order weighted essentially non-oscillatory schemes. *Journal of Scientific Computing* 67, 1 (2016), 299–323.
- [30] KUMAR, R., AND KADALBAJOO, M. Efficient high-resolution relaxation schemes for hyperbolic systems of conservation laws. *International Journal for Numerical Methods in Fluids* 55, 5 (2007), 483–507.
- [31] KURGANOV, A., AND TADMOR, E. Solution of two-dimensional riemann problems for gas dynamics without riemann problem solvers. *Numerical Methods for Partial Differential Equations* 18, 5 (sep 2002), 584–608.

- [32] LAX, P. D. Weak solutions of nonlinear hyperbolic equations and their numerical computation. *Communications on Pure and Applied Mathematics* 7, 1 (1954), 159–193.
- [33] LEFLOCH, P. G., MERCIER, J. M., AND ROHDE, C. Fully discrete, entropy conservative schemes of arbitrary order. *SIAM Journal on Numerical Analysis* 40, 5 (jan 2002), 1968–1992.
- [34] LEVEQUE, R. J. *Finite volume methods for hyperbolic problems*, vol. 31. Cambridge university press, 2002.
- [35] LISKA, R., AND WENDROFF, B. Comparison of several difference schemes on 1d and 2d test problems for the euler equations. *SIAM Journal on Scientific Computing* 25, 3 (2003), 995–1017.
- [36] LIU, Q., LIU, Y., AND FENG, J. The scaled entropy variables reconstruction for entropy stable schemes with application to shallow water equations. *Computers & Fluids* 192 (2019), 104266.
- [37] LIU, X.-D., OSHER, S., CHAN, T., ET AL. Weighted essentially non-oscillatory schemes. *Journal of computational physics* 115, 1 (1994), 200–212.
- [38] MAGNUS, J. R. On the concept of matrix derivative. *Journal of Multivariate Analysis* 101, 9 (2010), 2200–2206.
- [39] OSHER, S., AND CHAKRAVARTHY, S. High resolution schemes and the entropy condition. *SIAM Journal on Numerical Analysis* 21, 5 (1984), 955–984.
- [40] OSHER, S., AND CHAKRAVARTHY, S. Very high order accurate tvd schemes. In *Oscillation theory, computation, and methods of compensated compactness*. Springer, 1986, pp. 229–274.
- [41] PARVIN, S., AND KUMAR DUBEY, R. A new framework to construct third-order weighted essentially nonoscillatory weights using weight limiter functions. *International Journal for Numerical Methods in Fluids* 93, 4 (2021), 1213–1234.
- [42] RANOCHA, H. Comparison of some entropy conservative numerical fluxes for the euler equations. *Journal of Scientific Computing* 17 (2018), 216–242.
- [43] RATHAN, S., AND RAJU, G. N. A modified fifth-order weno scheme for hyperbolic conservation laws. *Computers & Mathematics with Applications* 75, 5 (2018), 1531–1549.
- [44] RUSANOV, V. V. Calculation of interaction of non-steady shock-waves with obstacles. *J. Comput. Math. Phys., USSR* (1961).
- [45] SANDERS, R. On convergence of monotone finite difference schemes with variable spatial differencing. *Mathematics of Computation* 40, 161 (1983), 91–106.
- [46] SCHULZ-RINNE, C. W., COLLINS, J. P., AND GLAZ, H. M. Numerical solution of the riemann problem for two-dimensional gas dynamics. *SIAM Journal on Scientific Computing* 14, 6 (1993), 1394–1414.
- [47] SERNA, S., AND MARQUINA, A. Power eno methods: a fifth-order accurate weighted power eno method. *Journal of Computational Physics* 194, 2 (2004), 632–658.
- [48] SHU, C.-W. Total-variation-diminishing time discretizations. *SIAM Journal on Scientific and Statistical Computing* 9, 6 (1988), 1073–1084.
- [49] SHU, C.-W. Essentially Non-Oscillatory and Weighted Essentially Non-Oscillatory Schemes for Hyperbolic Conservation Laws. Technical Report NASA/CR-97-206253, NAS 1.26:206253, ICASE-97-65, Institute for Computer Applications in Science and Engineering; Hampton, VA United States, 1997.
- [50] SHU, C. W. High order weighted essentially nonoscillatory schemes for convection dominated problems. *SIAM Review* 51, 1 (feb 2009), 82–126.

- [51] SHU, C.-W., AND OSHER, S. Efficient implementation of essentially non-oscillatory shock-capturing schemes. *Journal of Computational Physics* 77, 2 (1988), 439 – 471.
- [52] SOD, G. A. A survey of several finite difference methods for systems of nonlinear hyperbolic conservation laws. *Journal of computational physics* 27, 1 (1978), 1–31.
- [53] SWEBY, P. K. High resolution schemes using flux limiters for hyperbolic conservation laws. *SIAM journal on numerical analysis* 21, 5 (1984), 995–1011.
- [54] TADMOR, E. The numerical viscosity of entropy stable schemes for systems of conservation laws. i. *Math. Comp* 49 (1987), 91–103.
- [55] TADMOR, E. Convenient total variation diminishing conditions for nonlinear difference schemes. *SIAM journal on numerical analysis* 25, 5 (1988), 1002–1014.
- [56] TADMOR, E. Entropy stability theory for difference approximations of nonlinear conservation laws and related time-dependent problems. *Acta Numerica* 12 (may 2003), 451–512.
- [57] TADMOR, E. Perfect derivatives, conservative differences and entropy stable computation of hyperbolic conservation laws. *Discrete and Continuous Dynamical Systems* 36, 8 (mar 2016), 4579–4598.
- [58] TORO, E., AND BILLETT, S. J. Centred tvd schemes for hyperbolic conservation laws. *IMA Journal of Numerical Analysis* 20, 1 (2000), 47–79.
- [59] TORO, E. F. *Riemann solvers and numerical methods for fluid dynamics: a practical introduction*. Springer Science & Business Media, 2013.
- [60] WINTERS, A. R., AND GASSNER, G. J. Affordable, entropy conserving and entropy stable flux functions for the ideal mhd equations. *Journal of Computational Physics* 304 (2016), 72 – 108.
- [61] WOODWARD, P., AND COLELLA, P. The numerical simulation of two-dimensional fluid flow with strong shocks. *Journal of computational physics* 54, 1 (1984), 115–173.
- [62] ZAKERZADEH, H., AND FJORDHOLM, U. S. High-order accurate, fully discrete entropy stable schemes for scalar conservation laws. *IMA Journal of Numerical Analysis* (2015).
- [63] ZHANG, X., AND SHU, C.-W. A genuinely high order total variation diminishing scheme for one-dimensional scalar conservation laws. *SIAM Journal on Numerical Analysis* 48, 2 (2010), 772–795.
- [64] ZHANG, X., AND SHU, C.-W. Maximum-principle-satisfying and positivity-preserving high-order schemes for conservation laws: survey and new developments. *Proceedings: Mathematical, Physical and Engineering Sciences* 467, 2134 (2011), 2752–2776.